THE JOURNAL OF BIOLOGICAL CHEMISTRY VOL. 286, NO. 12, pp. 10316–10328, March 25, 2011

Identification of the Synthetic Cannabinoid *R*(+)WIN55,212-2 as a Novel Regulator of IFN Regulatory Factor 3 Activation and IFN-β Expression

RELEVANCE TO THERAPEUTIC EFFECTS IN MODELS OF MULTIPLE SCLEROSIS[*S]

Received for publication, September 24, 2010, and in revised form, January 17, 2011 Published, JBC Papers in Press, January 18, 2011, DOI 10.1074/jbc.M110.188599

Eric J. Downer[‡1], **Eileen Clifford**[‡1], **Bruno Gran**[§], **Hendrik J. Nel**[¶], **Padraic G. Fallon**[¶], **and Paul N. Moynagh**[‡2]

From the [‡]*Institute of Immunology, National University of Ireland Maynooth, Co. Kildare, Ireland, the* [§]*Division of Clinical Neurology, University of Nottingham, Nottingham, United Kingdom, and the* [¶]*Institute of Molecular Medicine, Trinity College Dublin, St. James's Hospital, Dublin 8, Ireland*

β-Interferons (IFN-βs) represent one of the first line treatments for relapsing-remitting multiple sclerosis, slowing disease progression while reducing the frequency of relapses. Despite this, more effective, well tolerated therapeutic strategies are needed. Cannabinoids palliate experimental autoimmune encephalomyelitis (EAE) symptoms and have therapeutic potential in MS patients although the precise molecular mechanism for these effects is not understood. Toll-like receptor (TLR) signaling controls innate immune responses and TLRs are implicated in MS. Here we demonstrate that the synthetic cannabinoid *R*(+)WIN55,212-2 is a novel regulator of TLR3 and TLR4 signaling by inhibiting the pro-inflammatory signaling axis triggered by TLR3 and TLR4, whereas selectively augmenting TLR3-induced activation of IFN regulatory factor 3 (IRF3) and expression of IFN-β. We present evidence that *R*(+)WIN55,212-2 strongly promotes the nuclear localization of IRF3. The potentiation of IFN-β expression by *R*(+)WIN55,212-2 is critical for manifesting its protective effects in the murine MS model EAE as evidenced by its reduced therapeutic efficacy in the presence of an anti-IFN-β antibody. *R*(+)WIN55,212-2 also induces IFN-β expression in MS patient peripheral blood mononuclear cells, whereas down-regulating inflammatory signaling in these cells. These findings identify *R*(+)WIN55,212-2 as a novel regulator of TLR3 signaling to IRF3 activation and IFN-β expression and highlights a new mechanism that may be open to exploitation in the development of new therapeutics for the treatment of MS.

IFN-β is one of several immunomodulatory drugs currently available to treat patients with relapsing-remitting MS[3] (1), displaying significant beneficial effects on disability progression (2) and relapse rate (3). The mechanism(s) of action of IFN-β is clearly complex with demonstrated effects on antigen presentation, co-stimulatory molecule expression, T-cell proliferation, and leukocyte migration (4). Despite its success in the clinic, IFN-β therapy has demonstrated partial efficacy along with various side effects (4), indicating a pressing need for more effective strategies.

Cannabis (*Cannabis sativa*) has a long history of consumption therapeutically (5). The term "cannabinoid" incorporates the active components of *C. sativa*, the plant-derived cannabinoids, the endogenous cannabinoids (endocannabinoids), and the synthetic cannabinoid ligands. Cannabinoids are used for the treatment/management of inflammatory conditions including MS (6), arthritis (7), and glaucoma (8). Indeed Sativex (a combination of two plant-derived cannabinoids, tetrahydrocannabinol and cannabidiol) is currently approved for the neuropathic pain and spasticity associated with MS (9). Despite the growing clinical use of cannabinoids their mechanism(s) of therapeutic action are not fully elucidated.

Cannabinoids elicit their effects via cannabinoid receptors (CB_1 and CB_2) (10, 11). However, some cannabinoid-induced effects are mediated independently of these receptors (12). Cannabinoid receptors are localized throughout the central nervous system (CNS) (13) and on immune cells associated with neuroinflammation (14). This is particularly relevant as cannabinoids therapeutically impact diseases associated with a dysregulation of the immune and nervous systems (13). Indeed in experimental autoimmune encephalomyelitis (EAE) cannabinoids attenuate the development of disease (15). The roles of $CB_{1/2}$ in mediating these effects varies depending on the pharmacological profile of the cannabinoid (16). Furthermore, whereas CB_1 confers neuroprotection in the CNS (17), the CB_2 receptor plays a pivotal protective role in the periphery by regulating T-cell effector function and myeloid progenitor trafficking into the CNS (16, 18).

TLRs are single transmembrane receptors involved in the recognition of bacterial/viral products and induce signaling involving the activation of transcription factors, such as NF-κB, and induction of genes encoding IFNs and cytokines (19). To

* This work was supported by Science Foundation Ireland (to P. N. M.), an IRCSET postdoctoral fellowship (to E. J. D.), and a research grant from the MS Society of Great Britain and Northern Ireland (to B. G.).

[S] The on-line version of this article (available at http://www.jbc.org) contains supplemental Figs. S1–S4.

[1] Both authors contributed equally to this work.

[2] To whom correspondence should be addressed. Tel.: 353-1-708-6105; Fax: 353-1-708-6337; E-mail: Paul.Moynagh@nuim.ie.

[3] The abbreviations used are: MS, multiple sclerosis; EAE, experimental autoimmune encephalomyelitis; BMDMs, bone marrow-derived macrophages; CB, cannabinoid receptor; IRF3, IFN regulatory factor 3; MyD88, myeloid differentiation factor 88; PBMCs, peripheral blood mononuclear cells; PLP, proteolipid protein; PTX, pertussis toxin; TBK1, TRAF family member-associated NF-κB activator (TANK)-binding kinase 1; TIR, Toll-interleukin-1 receptor; TLR, Toll-like receptor; TRIF, TIR-domain-containing adaptor-inducing interferon-β.

date, 13 mammalian TLRs have been identified, and with the exception of TLR3, all TLRs recruit the adaptor myeloid differentiation factor 88 (MyD88) (20). TLR3 (and TLR4) induces MyD88-independent signaling to regulate NF-κB via Toll-interleukin-1 receptor (TIR)-domain-containing adaptor-inducing IFN-β (TRIF) protein. Such TRIF-mediated signaling constitutes the MyD88-independent pathway and in addition to stimulating NF-κB, this pathway promotes phosphorylation of transcription factors IRF3 and IRF7, via two kinases, TRAF family member-associated NF-κB activator (TANK)-binding kinase 1 (TBK1) and inducible IκB kinase (21). The phosphorylation of IRF3/7 promotes their nuclear translocation and induction of type I IFNs (19). With respect to MS, specific roles of TLRs have been shown in EAE (22), with changes in TLR expression observed in MS brain lesions (23).

Because IL-1 signaling is sensitive to *R*(+)WIN55,212-2 (24) and the IL-1R and TLRs contain a homologous Toll/IL-1R (TIR) domain (25), we aimed to evaluate the effects of *R*(+)WIN55,212-2 on TLR signaling, with particular focus on the molecular mechanism controlling the induction of IFN-β. Protective roles in EAE have been demonstrated for TLR3 (26) and TLR4 (27) and thus we focused on the effects of *R*(+)WIN55,212-2 on these pathways. We show that whereas *R*(+)WIN55,212-2 negatively regulates the activation of NF-κB in response to TLR3/4, it enhances TLR3-induced IRF3 activation and IFN-β expression. We further show that *R*(+)WIN55,212-2-induced expression of IFN-β mediates its protective effects in EAE. Finally, evidence is presented that the positive effects of *R*(+)WIN55,212-2 on IFN-β is apparent in cells from MS patients. This study thus identifies a novel regulatory pathway that may be open to exploitation in the therapeutic treatment of MS.

EXPERIMENTAL PROCEDURES

Cell Culture—HEK293 cells stably expressing the TLR3 and TLR4 receptors were from InvivoGen (Toulouse, France). Human U373 astrocytoma cells stably transfected with *CD14* (U373-CD14) and bone marrow-derived macrophages (BMDMs) from wild type and TRIF-deficient mice were gifts from Dr. Katherine Fitzgerald (University of Massachusetts Medical School, Boston, MA). Cell lines were maintained in DMEM supplemented with 10% FBS, 100 μg/ml of penicillin, and 100 μg/ml of streptomycin. Cells were maintained in a 37 °C humidified atmosphere with 5% CO_2. The neomycin analog G418 (500 μg/ml) was used to select for the stably transfected TLR cell lines and maintenance of CD14 expression. Primary astrocytes were prepared as previously described (28) from the whole brain of 1-day-old C57/BL6 mice in accordance with the guidelines laid down by the local ethical committee (National University of Ireland, Maynooth). Briefly, astrocytes were isolated from mixed glia at days 10–14 by removing non-adherent cells with mechanical shaking and harvesting by trypsinization (0.25% trypsin, 0.02% EDTA). Cells were centrifuged (2,000 × *g* for 5 min at 20 °C) and the astrocyte-enriched pellet resuspended in DMEM. Astrocytes were plated (2×10^5 cells/ml) on 6- or 12-well plates and treated 24 h later. *R*(+)WIN55,212-2 and *S*(−)WIN55,212-2 (Sigma) were initially dissolved in DMSO and stored as 5 mM stock solutions. For culture use, the stock drug was diluted to a final concentration in culture medium and DMSO (≤0.1%) was used as vehicle control.

Patients and Blood Samples—Healthy donors and MS patients attending outpatient clinics at Queens Medical Centre University Hospital, University of Nottingham, UK, were recruited for this study. Written informed consent was obtained from each patient and the study received ethical approval from the Nottingham Research Ethics Committee. Patients with relapsing-remitting MS were clinically stable with an age ranging between 38 and 56 years (mean 48.4 ± 8.3; $n = 3$). Patients were naive to any disease modifying therapies including IFN-β, glatiramer acetate, and natalizumab. Healthy individuals were recruited from the University of Nottingham (mean age 31 ± 2.6; $n = 3$). Venous blood (30 ml) was obtained from each subject. PBMCs were isolated using the Ficoll-Hypaque isolation technique and plated (1×10^6 cells/ml) on 24-well plates.

Transient Transfections—HEK293 cells, U373-CD14 cells, and BMDMs (2×10^5 cells/ml) were seeded in 96-well plates and allowed to adhere for 24 h. Cells were transfected using Lipofectamine 2000 with firefly luciferase NF-κB reporter plasmids (κB-luc) (80 ng), constitutively expressed *Renilla* luciferase reporter construct (phRL-TK) (20 ng), IFN-β luciferase reporter construct (80 ng), positive regulatory domains I–III luciferase reporter construct (80 ng), and TRIF reporter constructs (50 ng). To measure the activation of IRF3, cells were transfected with pFR-Luc (60 ng) and the *trans*-activator plasmid pFA-IRF3 (IRF3 fused downstream of the yeast Gal4 DNA binding domain, 30 ng). To measure the activation of IRF7, cells were transfected with pFR-Luc (60 ng) and the *trans*-activator plasmid pFA-IRF7 (IRF7 fused downstream of the yeast Gal4 DNA binding domain, 25 ng). Cells were allowed to recover overnight and then pre-treated with or without *R*(+)WIN55,212-2 or *S*(-)WIN 55,212-2 for 1 h prior to stimulation in the presence or absence of the TLR4 agonist, LPS (100 ng/ml; Alexis Corporation, Lausen, Switzerland), or the TLR3 ligand, poly(I·C) (25 μg/ml; InvivoGen) for a further 4–6 h. Cell extracts were generated using the reporter lysis buffer (Promega, Southampton, UK) and extracts were assayed for firefly luciferase and *Renilla* luciferase activity using the luciferase assay system (Promega) and coelenterazine (1 μg/ml), respectively. Luminescence was monitored with a Glomax microplate luminometer (Promega). The *Renilla* luciferase plasmid was used to normalize for transfection efficiency in all experiments.

Induction and Assessment of EAE—EAE was induced in mice as described (29). Female SJL/J mice (8 weeks old) were injected subcutaneously at 2 sites, with 2 injections (100 μl) of emulsified Freund's complete adjuvant containing 100 μg of myelin proteolipid protein amino acids 139–151 (PLP-(139–151)) and 200 μg of *Mycobacterium tuberculosis* H37Ra followed 2 h later with 200 ng of pertussis toxin (PTX; Hooke Laboratories, Lawrence, MA) injected intraperitoneally. The preparation and immunization of the synthetic cannabinoid *R*(+)WIN55,212-2 (Sigma) was modified from previous studies (30). *R*(+)WIN55,212-2 was prepared in Cremophor El (Sigma) and PBS (20:80) and administered (20 mg/kg) intraperitoneally on

days 0, 1, 2, 3, 4, and 5. Rabbit anti-mouse IFN-β polyclonal antibody (Millipore, Cork, Ireland) was administered intraperitoneally (2×10^3 neutralizing units) on days 3 and 5 after PLP immunization. Control mice received Cremophor:PBS (20:80) as vehicle. Data are from 4 to 8 mice per group. To ensure objective clinical scoring, all mice had electronic data chips placed subcutaneously prior to the experiment and were subsequently tracked by barcode reader (AVID, UK). An investigator blinded to the treatment of the mice scored all animals by barcode number, to determine the mean clinical score as follows: 0, normal; 1, limp tail or hind limb weakness; 2, limp tail and hind limb weakness; 3, partial hind limb paralysis; 4, complete hind limb paralysis; and 5, moribund.

Histology—Spinal cords were dissected and fixed in 10% formaldehyde saline. Spinal cords were sectioned and stained with hematoxylin and eosin for inflammatory scoring (31). Inflammatory scores were as follows: 0, no inflammatory cells; 1, a few scattered inflammatory cells; 2, perivascular cuffing; 3, perivascular cuffing with extensions into adjacent parenchyma, or parenchymal infiltration without obvious cuffing. Demyelination was assessed on Luxol fast blue-stained spinal cord sections and scored as follows: 0, no evident demyelination; 1, decreased myelination with no foci; 2, obvious demyelination with evident foci; 3: severe demyelination. An investigator blinded to the treatment groups scored all stained sections, with slides labeled by mouse barcode number.

Western Immunoblotting—Astrocytes were seeded in 6-well plates (2×10^5 cells/ml). Cells were treated with poly(I·C) (25 μg/ml) for 5–360 min or pre-treated with *R*(+)WIN55,212-2 (20 μM) for 1 h prior to poly(I·C) (25 μg/ml) exposure for 1 h. Cells were then washed in ice-cold PBS before being lysed on ice for 10 min in 150 μl of lysis buffer (20 mM HEPES, pH 7.4, containing 10 mM KCl, 1.5 mM $MgCl_2$, 1 mM EDTA, 1 mM EGTA, 1 mM dithiothreitol, 0.1 mM PMSF, pepstatin A (5 μg/ml), leupeptin (2 μg/ml), and aprotinin (2 μg/ml)). Cell lysates were centrifuged at 13,000 × *g* for 15 min at 4 °C. The supernatant was mixed with SDS-PAGE sample buffer (0.125 Tris-HCl, pH 6.8, 20% (v/v) glycerol, 4% (w/v) SDS, 1.4 M β-mercaptoethanol, and 0.0025% (w/v) bromphenol blue). For *in vivo* experiments samples of spinal cord were homogenized in lysis buffer and the resulting lysate was centrifuged (16,000 × *g* for 15 min at 4 °C). Supernatants were then further centrifuged (100,000 × *g* for 1 h at 4 °C) and the supernatant (cytosolic fraction) added to sample buffer. All samples in sample buffer were boiled for 10 min and separated on 10% SDS-PAGE gels. Proteins were transferred to nitrocellulose membrane (Sigma) and blocked for 1 h in 5% dried milk. Membranes were incubated overnight at 4 °C with mouse monoclonal phospho-IκBα antibody (1:1,000 in 5% dried milk; Cell Signaling Technology Inc., Danvers, MA), rabbit monoclonal phospho-Ser^{396} IRF3 antibody (1:750 in 2.5% BSA; Cell Signaling Technology Inc.), rabbit monoclonal total IRF3 antibody (1:1,000 in 2.5% BSA; Cell Signaling Technology Inc.), or mouse monoclonal IκBα antibody (1:200 in 5% dried milk; Santa Cruz Biotechnology, Santa Cruz, CA). Membranes were washed and incubated with anti-mouse or anti-rabbit IRDye Infrared secondary antibody (1:5,000 in 5% dried milk; Licor Biosciences, Lincoln, NE) for 1 h in the dark at room temperature. The membranes were then washed and immunoreactive bands were detected using the Odyssey Infrared Imaging System (Licor Biosciences). Membranes were stripped and incubated with mouse monoclonal anti-β-actin antibody (1:10,000; overnight at 4 °C, Sigma). Molecular weight markers were used to calculate molecular weights of proteins represented by immunoreactive bands. Densitometry was performed using ImageJ software, and values were normalized for protein loading relative to levels of β-actin or total IRF3.

Preparation of Nuclear and Cytosolic Fractions—Primary astrocytes were seeded in 6-well plates (2×10^5 cells/ml). Cells were pre-treated with or without *R*(+)WIN55,212-2 (20 μM) for 1 h prior to stimulation in the absence or presence of poly(I·C) (25 μg/ml; 1 h). Cells were then washed in ice-cold PBS and scraped into 1 ml of ice-cold hypotonic buffer (10 mM HEPES-NaOH buffer, pH 7.9, containing 1.5 mM $MgCl_2$, 10 mM KCl, 0.5 mM DTT, and 0.5 mM PMSF). Cells were pelleted by centrifugation at 21,000 × *g* for 10 min and then lysed for 10 min on ice in hypotonic buffer (30 μl) containing 0.1% (v/v) Nonidet P-40. Lysates were centrifuged at 21,000 × *g* for 10 min. The resulting supernatants constituted cytosolic fractions and were measured for levels of IRF3 by Western immunoblotting. The pellets were resuspended in 20 mM HEPES-NaOH buffer, pH 7.9 (25 μl), containing 40 mM NaCl, 1.5 mM $MgCl_2$, 0.2 mM EDTA, 25% (w/v) glycerol, and 0.5 mM PMSF and incubated for 15 min on ice. Incubations were then centrifuged at 21,000 × *g* for 10 min, and the supernatants were removed into 10 mM HEPES-NaOH buffer, pH 7.9 (30 μl), containing 50 mM KCl, 0.2 mM EDTA, 20% (w/v) glycerol, 0.5 mM PMSF, and 0.5 mM DTT. Such samples constituted nuclear extracts and were assessed for levels of IRF3 by Western immunoblotting.

ELISA Detection of TNF-α and IL-8—U373-CD14 cells (2×10^5 cells/ml), primary astrocytes (2×10^5 cells/ml), and human PBMCs (1×10^6 cells/ml) were seeded in 96-, 12-, and 24-well plates, respectively. Cells were pre-treated with *R*(+)WIN55,212-2 (1–50 μM) for 1 h prior to LPS (100 ng/ml) or poly(I·C) (25 μg/ml) exposure for 6 h with the exception of PBMCs, which were pre-treated with *R*(+)WIN55,212-2 (20 μM) and *S*(−)WIN55,212-2 (20 μM) for 1 h prior to poly(I·C) (25 μg/ml) exposure for 3 h. Cell culture supernatants were assayed for levels of TNF-α and IL-8 by ELISA (Duoset, R&D Systems, Abingdon, UK).

Quantitative RT-PCR—HEK293 cells, U373-CD14 cells, BMDMs, primary astrocytes (all at 2×10^5 cells/ml), and human PBMCs (1×10^6 cells/ml) were seeded on 12-well plates. Cells were pre-treated with *R*(+)WIN55,212-2 or *S*(−)WIN55,212-2 (1–50 μM) for 1 h prior to LPS (100 ng/ml) or poly(I·C) (25 μg/ml) exposure for 4 h with the exception of PBMCs, which were pre-treated with *R*(+)WIN55,212-2 (20 μM) for 1 h prior to poly(I·C) (25 μg/ml) exposure for 3 h, and BMDMs, which were pre-treated with *R*(+)WIN55,212-2 (20 μM) for 1 h prior to poly(I·C) (25 μg/ml) exposure for 18 h. In some experiments cells were pre-treated with the CB_1 receptor antagonist SR141716 ((*N*-[piperidin-1-yl]-5-[4-chlorophenyl]-1-[2,4-dichlorophenyl]-4-methyl-1*H*-pyrazole-3-carboxamide), NIMH Chemical Synthesis Programme Batch 10937-163-1; 1 μM), the CB_2 receptor antagonist SR144528 ((*N*-[(1s)-endo-1,3,3-timethylbicyclo[2.2.1]heptan-2-yl]5-(4-choro-3-methyl-

panyl)-1-(4-methlbenzyl)pyrazole-3-carboxamide), Chemical Synthesis Programme: batch number 12687-177; 1 μM) or PTX (100 ng/ml, Sigma) prior to *R*(+)WIN55,212-2 or *S*(−)WIN55,212-2 exposure. RNA was extracted from cells and spinal cord using Tri Reagent™ (Invitrogen) and cDNA was generated from normalized RNA using SuperScript II reverse transcriptase. cDNA (1 μg) was amplified in the presence of SYBR® Green PCR master mix (New Engand Biolabs, Ipswich, MA). Primers used were as follows: murine *Ifn-β*, forward 5′-GGAGATGACGGAGAAGATGC-3′ and reverse 5′-CCCAGTGCTGGAGAAATTGT-3′; murine *Gfap*, forward 5′-GATCGCCACCTACAGGAAAT-3′ and reverse 5′-GTTTCTCGGATCTGGAGGTT-3′; murine *Cd11b*, forward 5′-CCTTGTTCTCTTTGATGCAG-3′ and reverse 5′-GTGATGACAACTAGGATCTT-3′; human *IFN-β*, forward 5′-GACCAACAAGTGTCTCCTCCAAA-3 and reverse ′5′-CTCCTCAGGGATGTCAAAGTTCA-3. As internal control murine *Gapdh*, forward 5′-AGGTCATCCCAGAGCTGAACG-3′ and reverse 5′-ACCCTGTTGCTGTAGCCGTA-3′ and human *HPRT*, forward 5′-TTGCTGACCTGCTGGATTAC-3′ and reverse 5′-TCTCCACCAATTACTTTTATGTCC-3′, were used in a similar reaction. Accumulation of gene-specific PCR products was measured continuously by means of fluorescence detection over 40 cycles. Samples were run in duplicate as follows: 10 min at 95 °C and for each cycle, 10 s at 95 °C, 10 s at 55 °C, and 1 min at 72 °C. Gene expression was calculated relative to the endogenous control and analysis was performed using the $2^{-\Delta\Delta C_T}$ method.

Screening of Cannabinoid Receptor Expression—Total cellular RNA was prepared from HEK293 cells, cDNA was generated as above and PCR amplification was performed to selectively amplify regions of CB_1, CB_2, and GAPDH cDNA.

cAMP Assay—HEK293 cells were pre-treated with or without PTX (100 ng/ml; 24 h), SR141716 (SR1; 1 μM for 1 h), and SR144528 (SR2; 1 μM for 1 h) prior to treatment with the selective CB_1 agonist ACEA (100 nM for 1 h; Tocris Bioscience, Bristol, UK) or the selective CB_2 agonist JWH133 (100 nM for 1 h; Sigma). Cells were then incubated with the potent cAMP phosphodiesterase inhibitor, 3-isobutyl-1-methylxanthine (500 μM for 15 min; Sigma) and stimulated with forskolin (30 μM for 30 min; Sigma) to induce cAMP. Lysates were harvested and assessed for levels of intracellular cAMP using a cAMP parameter kit as per the manufacturer's instructions (R&D Systems).

Confocal Microscopic Analysis of IRF3—For characterizaton of endogenous IRF3, primary astrocytes were seeded (1×10^5 cells/ml) in 4-well chamber slides (Lab-Tek, Roskilde, Denmark) and grown for 24 h. Cells were pre-treated with *R*(+)WIN55,212-2 (20 μM) or *S*(−)WIN55,212-2 (20 μM) for 1 h prior to poly(I·C) (25 μg/ml) exposure for 1 h. Cells were fixed in 4% paraformaldehyde, permeabilized with 0.2% Triton X-100 in PBS for 10 min at room temperature, and blocked with 10% goat serum (Vector Laboratories, Peterborough, UK) for 2 h. Cells were treated overnight at 4 °C with rabbit polyclonal IRF3 antibody (1:200 in 5% goat serum; Santa Cruz Biotechnology). Cells were washed and incubated with goat anti-rabbit Alexa 488 secondary antibody (1:500 in 5% goat serum; Invitrogen) and DAPI (1.5 μg/ml) in PBS, washed, and mounted (Vectashield, Vector Laboratories). All samples were viewed using an Olympus FluoView FV1000 confocal laser scanning microscope equipped with the appropriate filter sets. Acquired images were analyzed using the Olympus FV-10 ASW imaging software. Negative control experiments were performed by replacing the primary antibody with isotype controls (Millipore) and using equal gain settings during acquisition and analysis.

Statistical Analysis—Data are expressed as mean ± S.E., and the results represent two or three independent experiments. Statistical comparisons of different treatments were done by a one-way analysis of variance using a post hoc Student's Newman-Keuls test. Differences with a p value less than 0.05 were considered statistically significant.

RESULTS

R(+)WIN55,212-2 Regulates TLR3/4 Activation of NF-κB—We have shown that *R*(+)WIN55,212-2 targets the IL-1-induced transactivation of NF-κB in astrocytes (24). Because TLRs and IL-1R share signaling components (25), we extended our previous study to determine whether TLR signaling was sensitive to *R*(+)WIN55,212-2. TLR3 and TLR4 were targeted given their involvement in EAE (26) and evidence that their expression is up-regulated in MS lesions (23). Initial experiments assessed the ability of *R*(+)WIN55,212-2 to regulate NF-κB activity induced by TLR3 in response to poly(I·C) and by TLR4 in response to LPS in HEK293 cells. LPS and poly(I·C) enhanced expression of the NF-κB-regulated luciferase reporter gene, whereas *R*(+)WIN55,212-2 dose-dependently abrogated TLR4 (Fig. 1*A*) and TLR3 (Fig. 1*C*) NF-κB induction. The enantiomeric form of *R*(+)WIN55,212-2, *S*(−)WIN55,212-2, failed to affect the ability of LPS (Fig. 1*B*) and poly(I·C) (Fig. 1*D*) to activate NF-κB, suggesting that a stereoselective mechanism underlies the effects of *R*(+)WIN55,212-2.

Given the role of astrocytes in MS, in addition to NF-κB involvement in astrocyte-mediated neuroinflammation (32), we determined whether *R*(+)WIN55,212-2 could regulate TLR activation of NF-κB and the NF-κB responsive gene *Tnf-α* in astrocytes. Using astrocytoma U373 cells we demonstrated that *R*(+)WIN55,212-2 inhibited poly(I·C)- and LPS-induced activation of NF-κB and expression of TNF-α (supplemental Fig. S1). As a more physiologically relevant approach primary astrocytes were employed, and the regulatory effects of *R*(+)WIN55,212-2 were confirmed in these cells with dose-dependent inhibition of LPS- and poly(I·C)-induced TNF-α (Fig. 1, *E* and *G*). Again, stereoselectivity for this effect was confirmed (Fig. 1, *F* and *H*).

R(+)WIN55,212-2 Differentially Regulates TLR3/4 Induction of IRF3 and IFN-β—As MyD88 deficiency is protective in EAE (33), TRIF deficiency exacerbates the disease (34), we next delineated the sensitivity of MyD88-dependent and -independent signaling to cannabinoid exposure. As transcription factors IRF3 and IRF7 are activated by TLR3 and TLR4 in a MyD88-independent manner that employs TRIF (19), the sensitivity of IRF3/IRF7 to *R*(+)WIN55,212-2 was evaluated. Exposure of HEK293-TLR4 cells to LPS enhanced expression of IRF3-regulated luciferase and this was abrogated in a dose-dependent manner by *R*(+)WIN55,212-2 (Fig. 2*A*). In contrast,

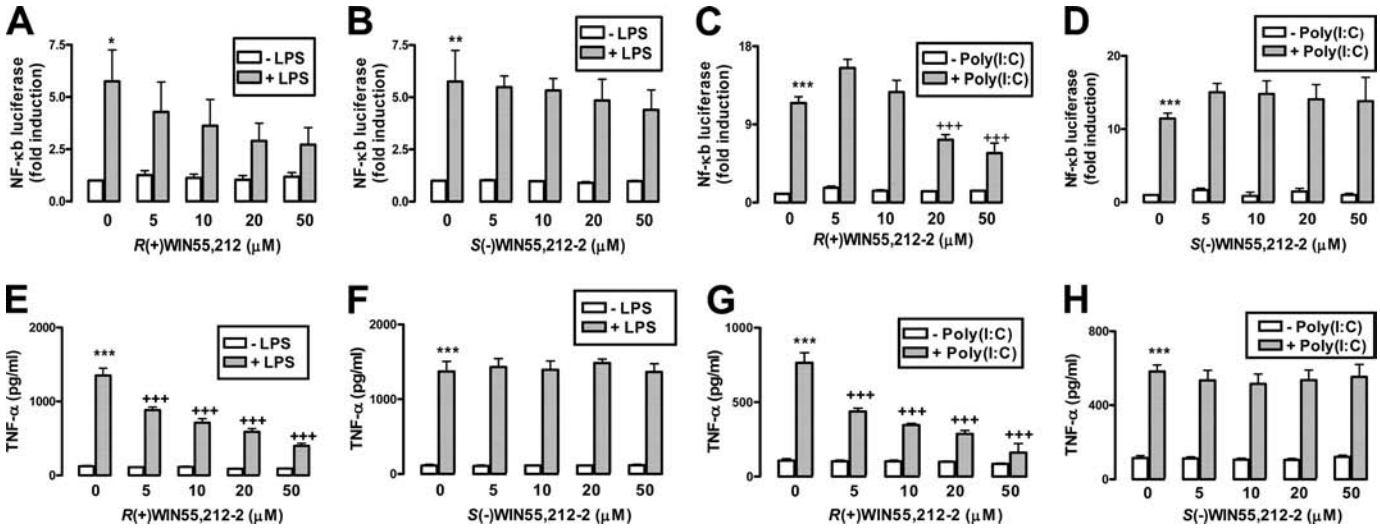

FIGURE 1. ***R*(+)WIN55,212-2 negatively regulates TLR3/4-induced activation of NF-κB and expression of TNF-α.** HEK293-TLR4 (*A* and *B*) and HEK293-TLR3 (*C* and *D*) cells were cotransfected with plasmids encoding NF-κB-regulated firefly luciferase (80 ng) and constitutively expressed TK *Renilla* luciferase (20 ng). 24 h post-transfection cells were treated in the absence or presence of *R*(+)WIN55,212-2 (5–50 μM) (*A*) and *S*(−)WIN55,212-2 (*B*) (5–50 μM) for 1 h prior to treatment with LPS (100 ng/ml) (*A* and *B*) and poly(I·C) (25 μg/ml) (*C* and *D*) for 6 h. Cell lysates were assayed for firefly luciferase activity and normalized for transfection efficiency using *Renilla* luciferase activity. Data are presented relative to vehicle-treated cells and represent the mean ± S.E. of triplicate determinations from three independent experiments. *E–H*, primary mouse astrocytes were seeded into 12-well plates, pre-treated with *R*(+)WIN55,212-2 (5–50 μM) (*E* and *G*) or *S*(−)WIN55,212-2 (5–50 μM) (*F* and *H*) for 1 h and stimulated with (*E* and *F*) LPS (100 ng/ml) or (*G* and *H*) poly(I·C) (25 μg/ml) for 6 h. Supernatants were analyzed for TNF-α production using sandwich ELISA. Data are presented as the mean ± S.E. of triplicate determinations from six animals and are representative of two independent experiments. *, $p < 0.05$; **, $p < 0.01$; and ***, $p < 0.001$ compared with vehicle-treated cells. +++, $p < 0.001$ compared with LPS- or poly(I·C)-treated cells.

R(+)WIN55,212-2, in a stereoselective manner, augmented poly(I·C)-induced activation of IRF3 in HEK293-TLR3 cells (Fig. 2, *B* and *C*), indicating that *R*(+)WIN55,212-2 differentially regulates TLR3- and TLR4-induced activation of IRF3. The synergistic effects of poly(I·C) and *R*(+)WIN55,212-2 were restricted to IRF3, because *R*(+)WIN55,212-2, in a stereoselective manner, inhibited LPS- (Fig. 2*D*) and poly(I·C)-induced (Fig. 2, *E* and *F*) IRF7-regulated luciferase. The selective augmentation by *R*(+)WIN55,212-2 of TLR-induced activation IRF3 is also apparent in astrocytoma cells (supplemental Fig. S2).

IRF3 is an important regulator of type I IFNs, including IFN-β (35). Because we demonstrated that *R*(+)WIN55,212-2 augments TLR3, but inhibits TLR4, activation of IRF3 (Fig. 2, *A* and *B*), we addressed the functional consequences of these effects of *R*(+)WIN55,212-2 on TLR3/TLR4 activation of the IFN-β promoter. Poly(I·C) activated the IFN-β promoter in HEK293-TLR3 (Fig. 2*G*) and U373-CD14 astrocytoma (Fig. 2*H*) cells with *R*(+)WIN55,212-2 potentiating this effect in both cell types. Such effects of *R*(+)WIN55,212-2 are mediated by targeting the IRF-binding enhancer element of the *IFN-β* promoter (termed the positive regulatory domains I-III) given that *R*(+)WIN55,212-2 augmented poly(I·C) induction of a reporter gene that is regulated exclusively by positive regulatory domains I-III (Fig. 2*I*). We next examined the effects of *R*(+)WIN55,212-2 on the expression of *Ifn-β* mRNA in BMDMs. Exposure of BMDMs to *R*(+)WIN55,212-2 alone caused some modest induction of *Ifn-β* mRNA with LPS and poly(I·C) showing much stonger levels of induction (Fig. 2, *J* and *K*). Interestingly *R*(+)WIN55,212-2 reduced LPS (Fig. 2*J*), but enhanced poly(I·C) (Fig. 2*K*) induction of *Ifn-β* mRNA. Similarly, exposure of primary astrocytes to *R*(+)WIN55,212-2 enhanced, in a stereoselective manner, poly(I·C)-induced expression of *Ifn-β* mRNA (supplemental Fig. S3, *A* and *B*).

R(+)WIN55,212-2 Augments TLR3-induced IRF3 Activation and IFN-β Induction in a Cannabinoid Receptor-independent Manner—We next characterized the cannabinoid pharmacology underlying the above effects. Receptor expression was first confirmed on HEK293 cells (Fig. 3*A*) and receptor involvement was addressed using the CB_1 and CB_2 antagonists, SR141716 and SR144528, respectively. Pre-exposure to SR141716 (Fig. 3, *B* and *C*) or SR144528 (Fig. 3, *D* and *E*), failed to attenuate the ability of *R*(+)WIN55,212-2 to potentiate poly(I·C)-induced activation of IRF3 (Fig. 3, *B* and *D*) and expression of *IFN-β* mRNA (Fig. 3, *C* and *E*). This indicates that *R*(+)WIN55,212-2 impacts the TLR3-IRF3-IFN-β axis independently of $CB_{1/2}$. Because $CB_{1/2}$ receptors signal via G_i proteins, we employed the G_i inhibitor PTX to validate this finding. PTX had no effect on the stimulatory effect of *R*(+)WIN55,212-2 on poly(I·C)-induced activation of IRF3 (Fig. 3*F*) and expression of IFN-β (Fig. 3*G*), confirming that *R*(+)WIN55,212-2 is acting in a cannabinoid receptor-independent manner. Both CB_1 and CB_2 antagonists and PTX were active in our system as they prevented the inhibitory effects of specific CB_1 and CB_2 agonists on forskolin-induced cAMP production (Fig. 3*H*).

The TLR3-TRIF-IRF3 Signaling Axis Is a Target for R(+)WIN55,212-2—We next defined the molecular target for *R*(+)WIN55,212-2 in the TLR3 pathway. TRIF was a primary target because it is a receptor proximal adaptor for TLR3 (36) and TRIF is protective in EAE (34). Overexpression of TRIF in HEK293 cells increased IRF3 luciferase activity (Fig. 4*A*); this was dose-dependently augmented by *R*(+)WIN55,212-2 (Fig. 4*A*) suggesting that TRIF-induced signaling is positively regulated by *R*(+)WIN55,212-2. TRIF-deficient cells were used to

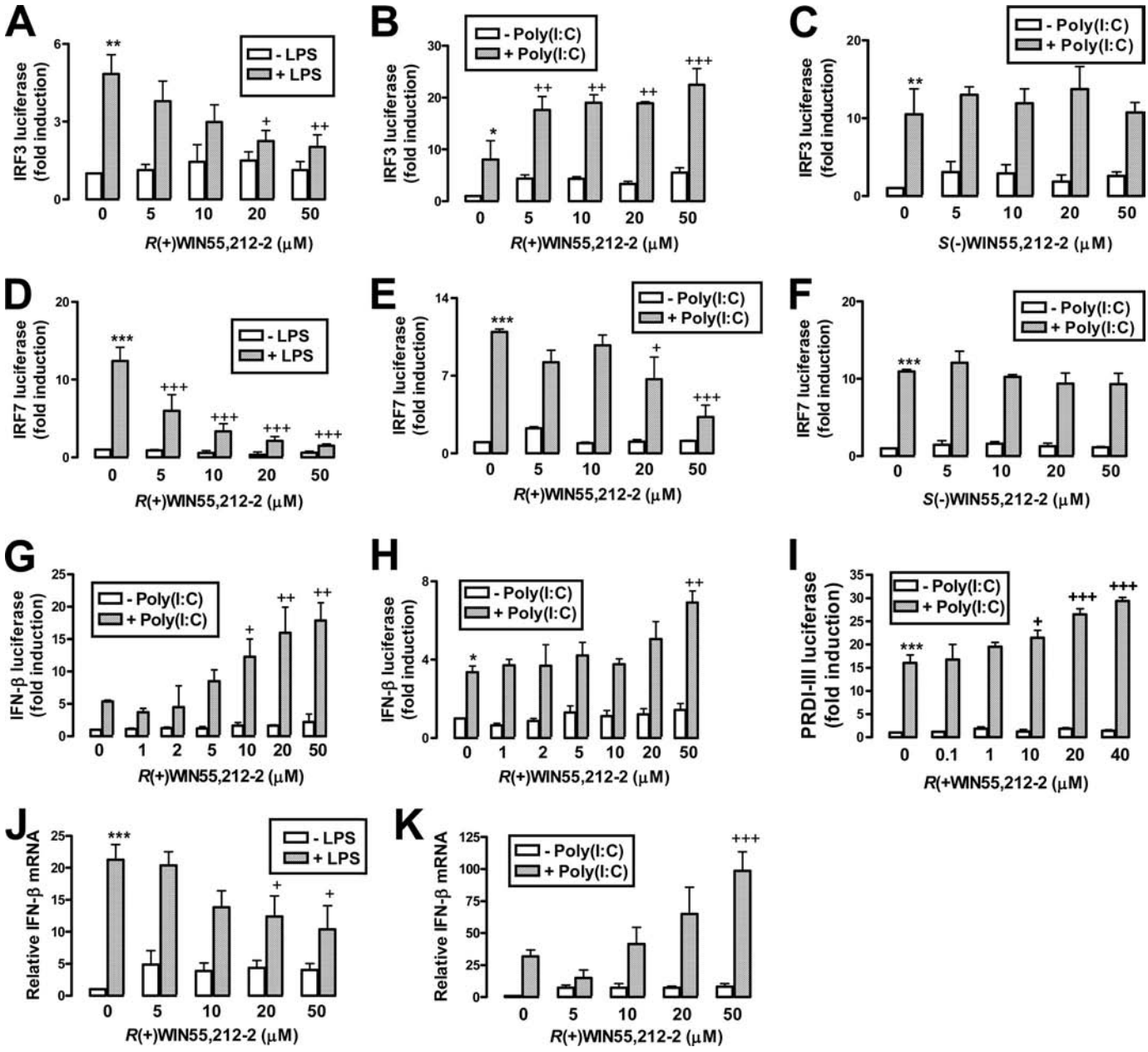

FIGURE 2. ***R*(+)WIN55,212-2 augments TLR3-induced activation of IRF3 and expression of IFN-β.** HEK293-TLR4 (*A*) and HEK293-TLR3 (*B* and *C*) cells were cotransfected with pFA-IRF3 (30 ng) and pFR-regulated firefly luciferase (60 ng) and constitutively expressed TK *Renilla* luciferase (20 ng). Transfected cells were left overnight and then cells were treated in the absence or presence of *R*(+)WIN55,212-2 (5–50 μM) (*A* and *B*) and *S*(−)WIN55,212-2 (5–50 μM) (*C*) for 1 h prior to treatment with/without LPS (100 ng/ml) (*A*) or poly(I·C) (25 μg/ml) (*B* and *D*) for 6 h. *D*, HEK293-TLR4, and HEK293-TLR3 (*E* and *F*) cells were cotransfected with pFA-IRF7 (25 ng) and pFR-regulated firefly luciferase (60 ng), left overnight, and treated in the absence or presence of *R*(+)WIN55,212-2 (5–50 μM) (*D* and *E*) and *S*(−)WIN55,212-2 (5–50 μM) (*F*) for 1 h prior to treatment with LPS (100 ng/ml) (*D*) or poly(I·C) (25 μg/ml) (*E* and *F*) for 6 h. HEK293-TLR3 (*G* and *I*) and U373-CD14 (*H*) cells were cotransfected with *IFN-β* promoter (*G* and *H*) or positive regulatory domains I-III-regulated firefly luciferase (80 ng) (*I*) and constitutively expressed TK *Renilla* luciferase (20 ng), left overnight, and treated in the absence or presence of *R*(+)WIN55,212-2 (1–50 μM) for 1 h prior to treatment with poly(I·C) (25 μg/ml) for 6 h. In all cases (*A–I*) cell lysates were assayed for firefly luciferase activity and normalized for transfection efficiency using *Renilla* luciferase activity and represent the mean ± S.E. of triplicate determinations from three independent experiments. *J* and *K*, BMDMs were treated in the absence or presence of *R*(+)WIN55,212-2 (5–50 μM) for 1 h prior to treatment with LPS (100 ng/ml) (*J*) or poly(I·C) (25 μg/ml) (*K*) for 18 h. cDNA was generated and assayed by quantitative real time PCR for levels of *Ifn-β* mRNA. The expression level of *Ifn-β* was normalized relative to expression of the housekeeping gene *Gapdh* and represent the mean ± S.E. of triplicate determinations from three independent experiments. *, $p < 0.05$; **, $p < 0.01$; and ***, $p < 0.001$ compared with vehicle-treated cells. +, $p < 0.05$; ++, $p < 0.01$; and +++, $p < 0.001$ compared with LPS- or poly(I·C)-treated cells.

evaluate the importance of TRIF for manifesting the effects of *R*(+)WIN55,212-2 on IFN-β. The responsiveness to poly(I·C) is greatly reduced in TRIF-deficient BMDMs with only modest induction of IFN-β in response to poly(I·C) observed (Fig. 4*B*). Interestingly, *R*(+)WIN55,212-2 failed to modulate this effect (Fig. 4*B*), further suggesting that *R*(+)WIN55,212-2 targets a TRIF-mediated pathway.

We next investigated if *R*(+)WIN55,212-2 directly targets IRF3. The phosphorylation of IRF3 is required for its dimerization and nuclear translocation (37). Poly(I·C) induced the time-

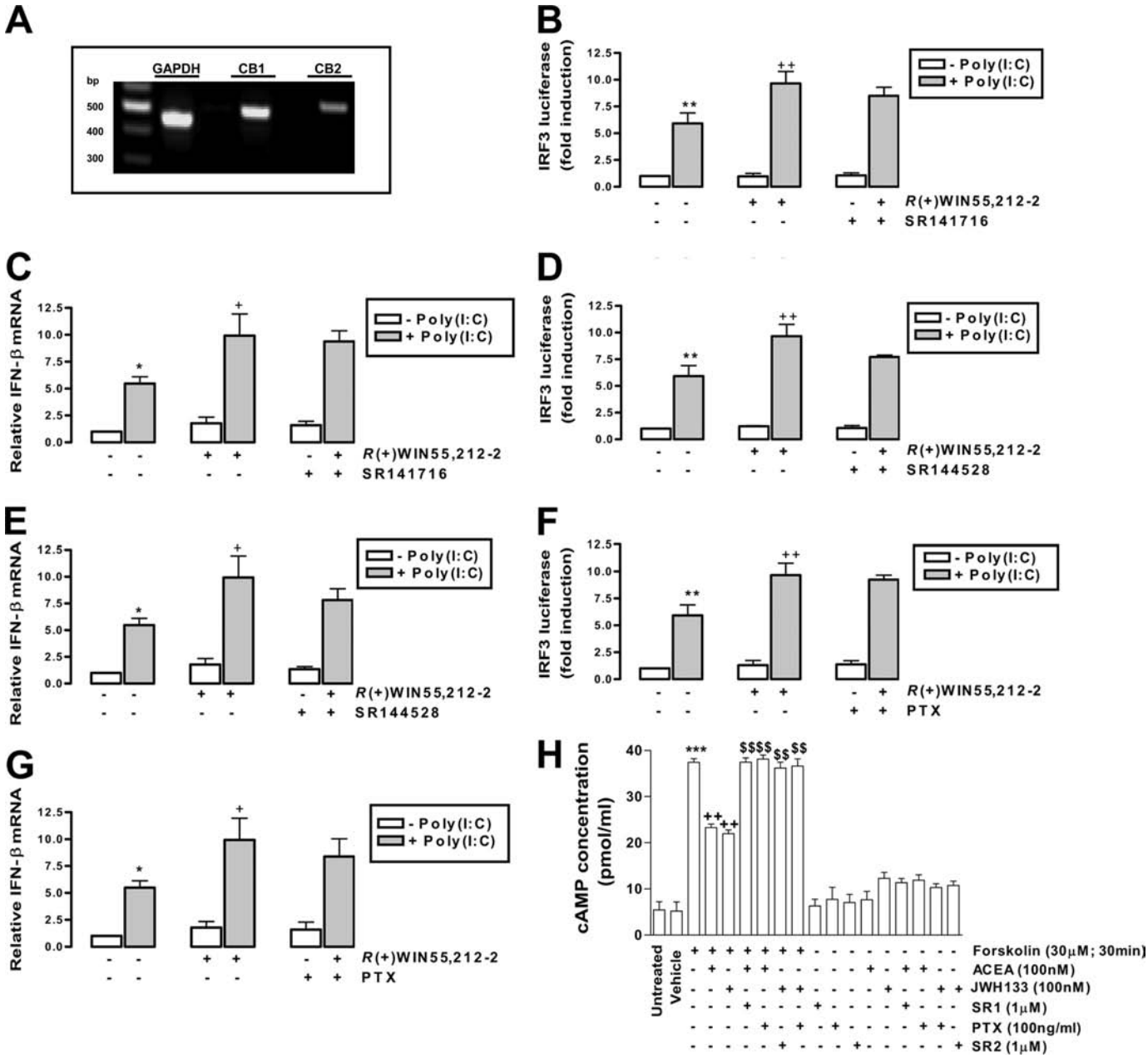

FIGURE 3. ***R*(+)WIN55,212-2 regulates TLR3 signaling in a cannabinoid receptor-independent manner.** *A*, total cellular RNA was prepared from HEK293 cells and subjected to first strand cDNA synthesis using SuperScript II reverse transcriptase and random oligonucleotide primers. PCR amplification was performed using *Taq* DNA polymerase and primers to selectively amplify regions of CB_1, CB_2, and *GAPDH* cDNA. *B, D,* and *F,* HEK293-TLR3 cells were cotransfected with pFA-IRF3 (30 ng) and pFR-regulated firefly luciferase (60 ng) and constitutively expressed TK *Renilla* luciferase (20 ng). Transfected cells were left overnight and then cells were pre-treated (1 h) with the inhibitors SR141716 (1 μM) (*B*), SR144528 (1 μM) (*D*), and PTX (50 ng/ml) (*F*) prior to exposure to *R*(+)WIN55,212-2 (20 μM; 1 h), and then stimulated with poly(I·C) (25 μg/ml) for 6 h. Cell lysates were assayed for firefly luciferase activity and normalized for transfection efficiency using *Renilla* luciferase activity. *C, E,* and *G*, HEK293-TLR3 cells were pre-treated (1 h) with the inhibitors SR141716 (1 μM) (*C*), SR144528 (1 μM) (*E*), and PTX (50 ng/ml) (*G*) prior to exposure to *R*(+)WIN55,212-2 (20 μM; 1 h), and then stimulated with poly(I·C) (25 μg/ml) for 4 h. cDNA was generated and assayed by quantitative real time PCR for levels of *IFN-β* mRNA. The expression level of *IFN-β* was normalized relative to expression of the housekeeping gene *GAPDH*. *H,* HEK293 cells were pre-treated with or without PTX (100 ng/ml; 24 h), SR141716 (*SR1*; 1 μM for 1 h), and SR144528 (*SR2*; 1 μM for 1 h) prior to treatment with ACEA (100 nM for 1 h) or JWH133 (100 nM for 1 h). Cells were then incubated with 3-isobutyl-1-methylxanthine (500 μM for 15 min) and stimulated with forskolin (30 μM for 30 min). Lysates were harvested and assessed for levels of intracellular cAMP using a cAMP parameter kit. Data represent the mean ± S.E. of triplicate determinations from three independent experiments. *, $p < 0.05$; **, $p < 0.01$; and ***, $p < 0.001$ compared with vehicle-treated cells. +, $p < 0.05$; and ++, $p < 0.01$ compared with poly(I·C)-treated cells (*B-G*) and forskolin-treated cells (*H*). $$, $p < 0.01$ compared with cells treated with ACEA/JWH133 in the presence of forskolin.

dependent phosphorylation of IRF3 in primary astrocytes (Fig. 4*C*) and *R*(+)WIN55,212-2 failed to modulate this phosphorylation (Fig. 4*D*). We next assessed the effects of *R*(+)WIN55,212-2 on subcellular localization of IRF3. IRF3 localizes predominantly to the cytoplasm, whereas poly(I·C) stimulation induces its nuclear translocation (Fig. 4, *E* and *F*). Intriguingly, *R*(+)WIN55,212-2 promoted nuclear localization of IRF3 in the presence and absence of poly(I·C) (Fig. 4, *E* and *F*), whereas the inactive enantiomer *S*(−)WIN55,212-2 is without effect (Fig. 4*E*). This effect was also confirmed in HEK293 cells

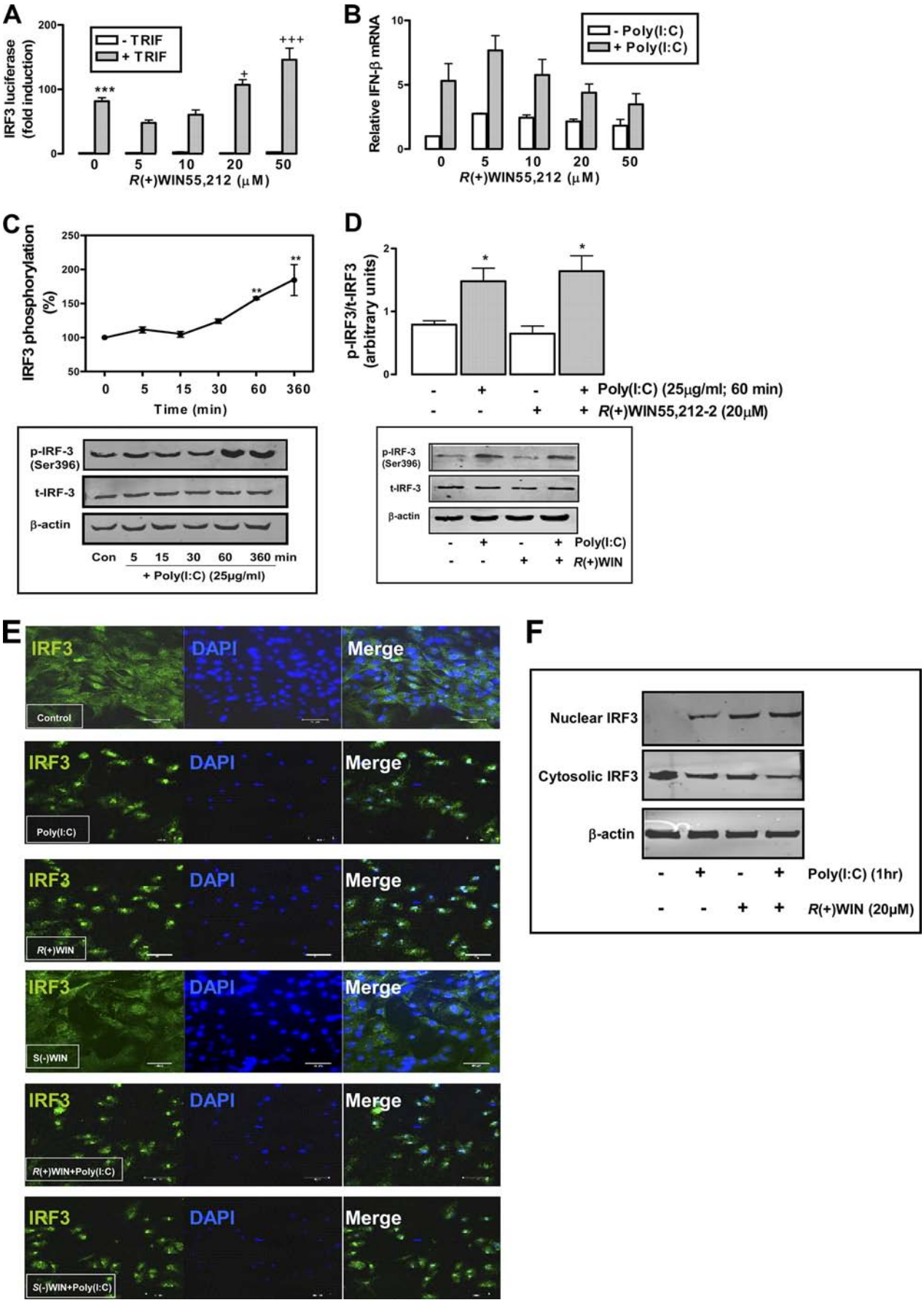

by demonstrating that *R*(+)WIN55,212-2 promotes the nuclear translocation of IRF3-GFP fusion protein (supplemental Fig. S4). The positive effects of *R*(+)WIN55,212-2 on the nuclear localization of IRF3 provides a plausible mechanistic basis to enhancement of the TLR3-TRIF-IRF3-IFN-β pathway.

R(+)WIN55,212-2 Manifests Protective Effects in EAE in an IFN-β-dependent Manner—Given the therapeutic effects of IFN-β in MS treatment it was attractive to speculate that *R*(+)WIN55,212-2 exerts its therapeutic properties in animal MS models by inducing endogenous IFN-β (26). A relapsing mouse model of EAE involving immunization with PLP-(139–151) (PLP) was employed to address this hypothesis. PLP-immunized mice develop clinical symptoms of disease from day 5 post-immunization, with disease severity peaking on day 16 followed by a relapse on day 26 (Fig. 5*A*). Mice treated with *R*(+)WIN55,212-2 showed delayed development of EAE and attenuated disease severity (Fig. 5*A*). However, PLP-immunized mice treated with *R*(+)WIN55,212-2 and an anti-IFN-β antibody were not protected (Fig. 5*A*). Scoring of histology sections confirmed *R*(+)WIN55,212-2 reduced lymphocytic infiltration (Fig. 5, *B* and *C*) and demyelination of spinal cords (Fig. 5*D*). However, anti-IFN-β ablated these protective effects (Fig. 5, *B–D*). Animals that received anti-IFN-β antibody alone displayed a similar degree of inflammation (Fig. 5*C*) and demyelination (Fig. 5*D*) as vehicle-treated mice.

We also characterized the effects of *R*(+)WIN55,212-2 on astrogliosis/microglial activation in PLP-immunized mice. *R*(+)WIN55,212-2 attenuated both GFAP mRNA (Fig. 5*E*) and CD11b mRNA (Fig. 5*F*) in EAE spinal cord, and this was reversed by anti-IFN-β. Finally, to characterize the anti-inflammatory effects of *R*(+)WIN55,212-2 at the molecular level, IκB proteins in spinal cords were analyzed. IκB proteins regulate NF-κB by sequestering NF-κB in the cytoplasm (38) with NF-κB activation dependent on phosphorylation and degradation of IκB. *R*(+)WIN55,212-2 reduced IκBα phosphorylation and IκBα degradation associated with EAE, and these effects were reversed by anti-IFN-β (Fig. 5*G*). This provides strong evidence that IFN-β plays a role in the protective effects of *R*(+)WIN55,212-2 in EAE.

Effect of R(+)WIN55,212-2 on IFN-β Expression in Human PBMCs—Because *R*(+)WIN55,212-2 augments IFN-β and its protective effects in EAE are IFN-β-dependent, we determined if *R*(+)WIN55,212-2 modulated IFN-β production in cells from MS patients. Indeed a defect in IFN-β production has been reported in immune cells from MS patients (39). PBMCs isolated from healthy subjects were responsive to poly(I·C) with an increase in *IFN-β* mRNA observed, whereas *R*(+)WIN55,212-2 ablated this (Fig. 6*A*). In contrast, PBMCs isolated from MS subjects were unresponsive to poly(I·C) with no *IFN-β* mRNA detected (Fig. 6*B*). Remarkably, cells from MS subjects displayed sensitivity to *R*(+)WIN55,212-2, with *R*(+)WIN55,212-2 robustly inducing *IFN-β* mRNA in the absence of poly(I·C) (Fig. 6*B*). Again, the enantiomeric form of *R*(+)WIN55,212-2, *S*(−)WIN55,212-2, had no effect on IFN-β expression profile in healthy (Fig. 6*C*) and MS patient (Fig. 6*D*) cells. These findings are significant given that plasmacytoid dendritic cells from MS patients produce lower levels of type I IFN (40) and are weakly responsive to IFN-β-induced maturation (41). The differential sensitivity of cells from healthy and MS subjects appear to be specific for IFN-β, because *R*(+)WIN55,212-2 blocks poly(I·C)-induced expression of TNF-α and IL-8 in PBMCs from both healthy (Fig. 6, *E* and *G*) and MS (Fig. 6, *F* and *H*) subjects. It is worth noting that paradoxically the *R*(+)WIN55,212-2-induced expression of IFN-β in MS cells is inhibited by poly(I·C), suggesting that TLR3 stimulation of MS cells drives a desensitizing signal. The induction of *IFN-β* mRNA in cells from MS patients by *R*(+)WIN55,212-2, coupled to the central role of IFN-β in mediating the protective effects of *R*(+)WIN55,212-2 in EAE, identifies a regulatory pathway that may be a valuable target in the design of new therapeutics to treat MS.

DISCUSSION

Here we aimed to understand the molecular mechanisms of the immunomodulatory effects of the cannabinoid *R*(+)WIN55,212-2 and in so doing we have identified an important regulatory pathway that may be able to control pathogenesis in MS. We propose that *R*(+)WIN55,212-2 controls the expression of IFN-β. In addition to ameliorating pro-inflammatory signaling induced by TLR3/4, *R*(+)WIN55,212-2 augments TLR3 signaling, enhancing IFN-β expression that ameliorates the pathology associated with EAE. We also demonstrate that cells from MS patients are especially sensitive to *R*(+)WIN55,212-2 in terms of increased expression of endog-

FIGURE 4. ***R*(+)WIN55,212-2 augments the TLR3/TRIF/TBK1 signaling axis and promotes nuclear localization of IRF3.** *A,* HEK293-TLR3 cells were cotransfected with pFA-IRF3 (30 ng), pFR-regulated firefly luciferase (60 ng), TRIF reporter constructs (50 ng), and constitutively expressed TK *Renilla* luciferase (20 ng). Transfected cells were left overnight and treated in the absence or presence of *R*(+)WIN55,212-2 (5–50 μM) for 6 h. Cell lysates were assayed for firefly luciferase activity and normalized for transfection efficiency using *Renilla* luciferase activity. Data are presented relative to vehicle-treated cells and represent the mean ± S.E. of triplicate determinations from three independent experiments. *B,* TRIF-deficient BMDMs were pre-treated (1 h) with *R*(+)WIN55,212-2 (20 μM) and then stimulated with poly(I·C) (25 μg/ml) for 18 h. cDNA was generated and assayed by quantitative real time PCR for levels of *Ifn-β* mRNA. The expression level of *Ifn-β* was normalized relative to expression of the housekeeping gene *Gapdh* and represents the mean ± S.E. of triplicate determinations from three independent experiments. *C* and *D,* primary mouse astrocytes were seeded into 6-well plates and treated with poly(I·C) (25 μg/ml) (*C*) for various time points (5–360 min) or pre-treated with *R*(+)WIN55,212-2 (20 μM; 1 h) (*D*) prior to stimulation with poly(I·C) (25 μg/ml) for 1 h. Cell lysates were subsequently subjected to Western immunoblotting using anti-phospho-Ser^{396} IRF3, anti-total IRF3, and anti-β-actin antibodies (*lower panels*). All immunoblots were subjected to densitometric analysis with levels of phospho-IRF3 normalized to total levels of IRF3 (*upper panels*). Densitometic data are representative of 8 (*C*) and 6 (*D*) independent experiments. *, $p < 0.05$; **, $p < 0.01$; and ***, $p < 0.001$ *versus* non-transfected (*A*) and vehicle-treated cells (*C* and *D*). +, $p < 0.05$; and +++, $p < 0.001$ compared with vehicle treated TRIF-transfected cells. *E,* primary mouse astrocytes were grown in chamber slides and pre-treated (1 h) with *R*(+)WIN55,212-2 (20 μM) or *S*(−)WIN55,212-2 (20 μM) for 1 h prior to poly(I·C) (25 μg/ml) exposure for 1 h. Cells were fixed, mounted in anti-fade medium with DAPI, and visualized using confocal microscopy. Confocal images were captured using a UV Zeiss 510 Meta System laser scanning microscope equipped with the appropriate filter sets. Data analysis was performed using the LSM 5 browser imaging software. Images are representative of three independent experiments. *Scale bars* are 20 μm. *F,* primary astrocytes were pre-treated with or without *R*(+)WIN55,212-2 (20 μM) for 1 h prior to stimulation in the absence or presence of poly(I·C) (25 μg/ml; 1 h). Cytosolic and nuclear fractions were prepared and subsequently subjected to Western immunoblotting using anti-total IRF3 and anti-β-actin antibodies. Blots are representative of data obtained from 6 animals.

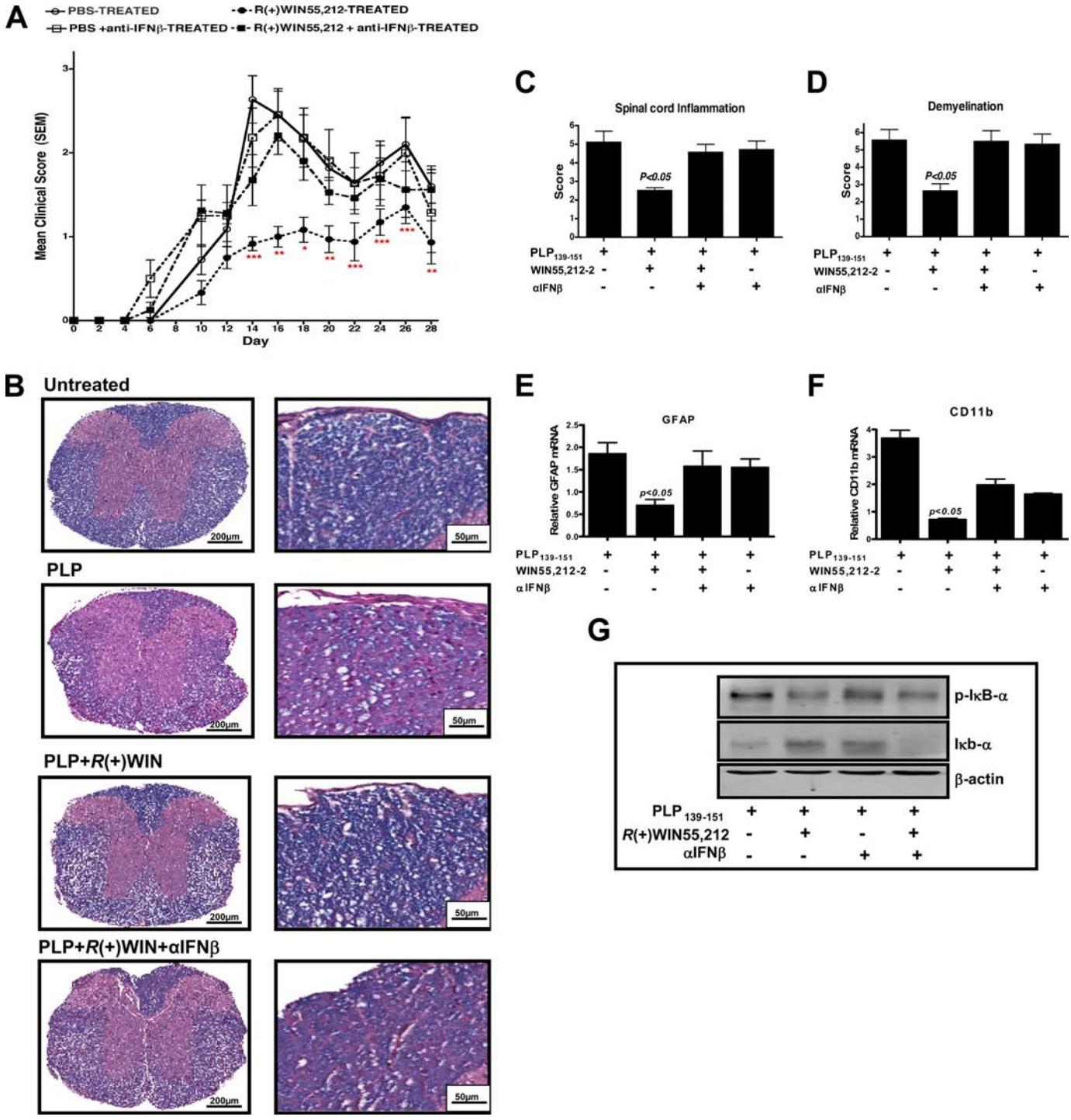

FIGURE 5. **Protective effects of *R*(+)WIN55,212-2 in EAE are mediated by IFN-β.** *A*, PLP-immunized mice develop clinical symptoms of EAE from day 5 post-immunization, with disease severity peaking on day 16 followed by a relapse on day 26. Mice treated with *R*(+)WIN55,212-2 (administered (20 mg/kg) intraperitoneally on days 0, 1, 2, 3, 4, and 5 after immunization) showed delayed development of EAE and attenuated disease severity. PLP-immunized mice treated with *R*(+)WIN55,212-2 and an anti-IFN-β antibody (administered intraperitoneally (2×10^3 neutralizing units) on days 3 and 5 after PLP immunization) were not protected. *B*, representative images of Luxol fast blue-stained spinal cord sections from untreated mice, PLP-treated, PLP + WIN-treated, and PLP + WIN + αIFNβ-treated mice illustrating the extent of demyelination and lymphocytic inflammation. The posterior funiculi of the spinal cord were observed under high power (*right panels*). Images are representative of data from 4 to 8 animals per treatment group. *Scale bars* are 200 and 50 μm. Spinal cords were sectioned and stained with hematoxylin and eosin and quantified for spinal cord inflammation (*C*) and extent of demyelination (*D*) using Luxol fast blue-stained spinal cord sections in treated groups. cDNA was generated from spinal cords and assayed by quantitative real time PCR for relative levels of *Gfap* mRNA (*E*) and *Cd11b* mRNA (*F*) from vehicle-treated, PLP-treated, PLP + WIN-treated, and PLP + WIN + αIFNβ-treated mice. The expression level of *Gfap* and *Cd11b* was normalized relative to expression of the housekeeping gene *Gapdh* and represent the mean ± S.E. of triplicate determinations from 4 to 8 animals per treatment group. Cytosolic fractions were prepared from the spinal cord of vehicle-treated, PLP-treated, PLP + WIN-treated, and PLP + WIN + αIFNβ-treated mice. Cell lysates were subsequently subjected to Western immunoblotting using anti-phospho IκBα, anti-total IκBα, and anti-β-actin antibodies. Blots are representative of data from 4 to 8 animals per treatment group. *, $p < 0.05$; **, $p < 0.01$; and ***, $p < 0.001$ for differences between WIN-treated mice and other groups.

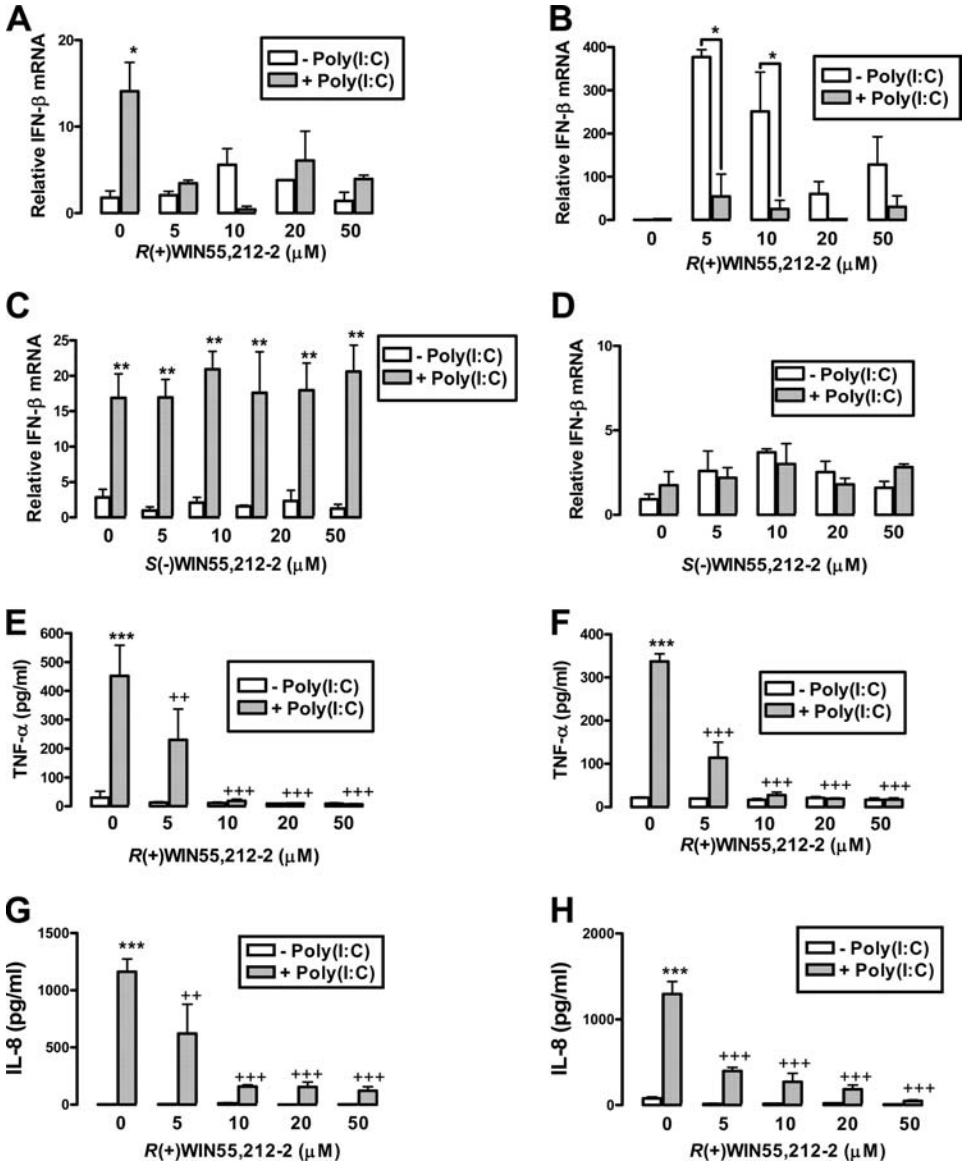

FIGURE 6. ***R*(+)WIN55,212-2 induces IFN-β expression in PBMCs from MS subjects.** *A–H*, PBMCs prepared from healthy subjects (*A, C, E,* and *G*) and MS patients (*B, D, F,* and *H*) were seeded into 24-well plates, pre-treated with *R*(+)WIN55,212-2 or *S*(−)WIN55,212-2 (5–50 μM) for 1 h, and stimulated with poly(I·C) (25 μg/ml) for 3 h. *A–D*, cDNA was generated and assayed by quantitative real time PCR for relative levels of *IFN-β* mRNA. The expression level of IFN-β was normalized relative to expression of the housekeeping gene *GAPDH* and represent the mean ± S.E. of triplicate determinations from three patients. Supernatants were analyzed for TNF-α (*E* and *F*) and IL-8 (*G* and *H*) production using sandwich ELISA. Data are presented as the mean ± S.E. of triplicate determinations from three patients. *, $p < 0.05$; **, $p < 0.01$; and ***, $p < 0.001$ compared with vehicle-treated cells (*A, C, E, F, G,* and *H*) or cells treated with *R*(+)WIN55,212-2 in the presence of poly(I·C) (*B*). ++, $p < 0.01$, and +++, $p < 0.001$ compared with poly(I·C)-treated cells.

enous IFN-β and this strongly indicates the mechanism described has relevance to treatment of MS.

The study highlights the anti-inflammatory potential of *R*(+)WIN55,212-2 by virtue of its inhibitory effects on the NF-κB pathway. We have previously shown that *R*(+)WIN55,212-2 blocks the IL-1 pathway leading to NF-κB (24) and here we demonstrate for the first time that it can inhibit TLR3/4-induced activation of NF-κB. This likely makes a major contribution to the inhibitory effects of *R*(+)WIN55,212-2 on pro-inflammatory gene expression. Indeed, we demonstrate that *R*(+)WIN55,212-2 blunts TLR3/4 induction of TNF-α. Such effects translate into strong anti-inflammatory activity *in vivo*. Thus *R*(+)WIN55,212-2 blunts neutrophil migration in a mouse peritonitis model (42), whereas *R*(+)WIN55,212-2 abrogates the clinical development of EAE (30). The inhibitory effects of *R*(+)WIN55,212-2 on leukocyte adhesion to endothelia is likely to contribute to its therapeutic properties in EAE (43). However, whereas these direct anti-inflammatory effects of *R*(+)WIN55,212-2 are pivotal, the present study highlights a novel mechanistic basis to its protective effects by virtue of its ability to induce endogenous IFN-β.

We provide evidence for the first time that IRF3 is a target for synthetic cannabinoids. We propose that *R*(+)WIN55,212-2 can enhance IRF3 nuclear localization and positively impact on IFN-β expression in response to TLR3 signaling. Intriguingly, *R*(+)WIN55,212-2 exerts differential effects on LPS- and poly(I·C)-induced activation of IRF3 and expression of IFN-β.

The mechanistic basis to this remains to be delineated. However, it has recently been shown that the TIR adaptor Mal, which is employed by TLR4 but not TLR3, can negatively regulate the induction of IFN-β (44) and it is interesting to speculate that Mal may mask any positive effects of *R*(+)WIN55,212-2 on TLR4 signaling. Furthermore, TLR3 signaling to NF-κB and IRF3 is differentially sensitive to *R*(+)WIN55,212-2 suggesting that the latter targets a component of the IRF pathway not common to the NF-κB pathway. Data presented herein suggest that *R*(+)WIN55,212-2 targets IRF3 and promotes its nuclear localization. It should be noted that the increased nuclear localization of IRF3 in response to *R*(+)WIN55,212-2 may reflect increased nuclear translocation and/or nuclear sequestration of IRF3. Indeed it is plausible that *R*(+)WIN55,212-2 may have a nuclear target that sequesters IRF3 and it is especially interesting to note that cannabinoids have previously been shown to be capable of targeting the nuclear peroxisome proliferator-activated receptors (45). Indeed a nuclear target for *R*(+)WIN55,212-2 may potentially explain why it positively regulates IRF3 in response to poly(I·C) and yet inhibits IRF7 activation in response to the same stimulus. Given that IRF3 and IRF7 tend to share the same upstream regulators the differential sensitivity of these two transcription factors to *R*(+)WIN55,212-2 suggest that IRF3 may itself be targeted by *R*(+)WIN55,212-2 and its effector molecules leading to increased nuclear localization, whereas IRF7 is not targeted by this process but instead is subject to another form of regulation that results in its inhibition. Indeed the NF-κB pathway is also subject to negative regulation by *R*(+)WIN55,212-2 and we have previously provided evidence that it targets the transactivation capacity of NF-κB (24). *R*(+)WIN55,212-2 may similarly regulate the transactivation potential of IRF7 and this is consistent with the presently described inhibitory effects of *R*(+)WIN55,212-2 on the transactivating ability of the Gal4-IRF7 fusion protein.

The concentrations of *R*(+)WIN55,212-2 used are in line with those used in various anti-inflammatory paradigms *in vitro* (46–48). Furthermore, the dose (30, 49, 50) and route of administration (30, 43, 49) for our *in vivo* experiments are comparable with the therapeutic doses used in these animal studies. The effects of *R*(+)WIN55,212-2 cannot be explained by mere virtue of its lipophilic characteristics because its enantiomeric form *S*(-)WIN55,212-2 is ineffective in our studies. *R*(+)WIN55,212-2 binds to both CB_1 and CB_2, however, use of selective $CB_{1/2}$ antagonists and PTX failed to inhibit the effect of *R*(+)WIN55,212-2 on IRF3 and IFN-β, suggesting that *R*(+)WIN55,212-2 is acting in a cannabinoid receptor-independent manner. Indeed, both CB_1 (24) and CB_2 (46) independent effects of *R*(+)WIN55,212-2 have been demonstrated, which further suggests the existence of additional cannabinoid receptors with some evidence that cannabinoids may act on peroxisome proliferator-activated receptors (45). Furthermore, the inability of the enantiomeric form of *R*(+)WIN55,212-2 to mimic its effects argues for a stereoselective receptor-mediated process(es).

This study highlights the importance of IFN-β production as a mechanism underlying the protective effects of *R*(+)WIN55,212-2 in EAE. We propose that such effects are due to a combination of neuroprotection and dampening of inflammation. Whereas, it is clear that the anti-inflammatory properties of *R*(+)WIN55,212-2 may be manifested directly by its effects on NF-κB, it is also apparent that the *in vivo* anti-inflammatory effects of *R*(+)WIN55,212-2 are dependent on IFN-β and the immunomodulatory potential of the latter. Such direct and indirect acting mechanisms of *R*(+)WIN55,212-2 may combine to explain its strong anti-inflammatory propensity.

Our studies also probed the effects of *R*(+)WIN55,212-2 on IFN-β in PBMCs and the findings raise intriguing issues. PBMCs from healthy donors responded to TLR3 stimulation by enhancing IFN-β production. Interestingly, this was absent in MS patient PBMCs, suggesting that the TLR3 pathway may be desensitized, at least with respect to IFN-β induction. Indeed viral involvement in MS manifestation has been demonstrated (51), and it is interesting to speculate that MS patients may be pre-sensitized to viral infection showing some form of TLR3 tolerance. Intriguingly, the non-responsiveness of MS patient PBMCs to poly(I·C) is only relevant in the context of IFN-β induction because poly(I·C) shows comparable efficacy in inducing TNF-α and IL-8 in cells from healthy and MS patients. Thus any form of TLR3 tolerance that may exist appears to be restricted to the pathway leading to IFN-β and this may explain why exogenous administration of IFN-β is effective in the treatment of MS. Remarkably, *R*(+)WIN55,212-2 alone induced the expression of IFN-β in PBMCs from MS patients. Thus whatever the basis underlying the refractory nature of MS cells to TLR3-induced IFN-β expression, *R*(+)WIN55,212-2 can bypass this blockage. This argues strongly in favor of the therapeutic potential of *R*(+)WIN55,212-2 in MS and presents an additional novel therapeutic strategy to the current exogenous administration of IFN-β. Intriguingly the induction of IFN-β by *R*(+)WIN55,212-2 in PBMCs from MS patients is strongly inhibited by poly(I·C). This suggests that the stimulation of TLR3 in cells from MS patients generates a negative input on IFN-β expression and is consistent with suggestions that viral infection can exacerbate disease.

Although cannabinoids show promising therapeutic effects in EAE models and MS patients, their mechanism(s) of action are poorly understood. We present a novel insight into the molecular basis underlying their therapeutic properties. We suggest that the innate arm of the immune response is a target for cannabinoid anti-inflammatory action and highlight a novel dual mechanism of action of *R*(+)WIN55,212-2. First, it can exert anti-inflammatory properties by down-regulating TLR-induced activation of NF-κB and induction of pro-inflammatory mediators. In parallel, by enhancing activation of IRF3 and induction of IFN-β it can boost an endogenous protective system. Such effects of *R*(+)WIN55,212-2, in particular its capacity to induce endogenous IFN-β, offers an attractive additional option to the current use of exogenously administered IFN-β.

REFERENCES

1. Goodin, D. S., and Bates, D. (2009) *Mult. Scler.* **15,** 1175–1182
2. Jacobs, L. D., Cookfair, D. L., Rudick, R. A., Herndon, R. M., Richert, J. R., Salazar, A. M., Fischer, J. S., Goodkin, D. E., Granger, C. V., Simon, J. H., Alam, J. J., Bartoszak, D. M., Bourdette, D. N., Braiman, J., Brownscheidle, C. M., Coats, M. E., Cohan, S. L., Dougherty, D. S., Kinkel, R. P., Mass,

M. K., Munschauer, F. E., 3rd, Priore, R. L., Pullicino, P. M., Scherokman, B. J., Whitham, R. H., *et al.* (1996) *Ann. Neurol.* **39,** 285–294
3. Li, D. K., and Paty, D. W. (1999) *Ann. Neurol.* **46,** 197–206
4. Vosoughi, R., and Freedman, M. S. (2010) *Clin. Neurol. Neurosurg.* **112,** 365–385
5. Ashton, J. C. (2007) *Curr. Opin. Investig. Drugs* **8,** 373–384
6. Wade, D. T., Makela, P., Robson, P., House, H., and Bateman, C. (2004) *Mult. Scler.* **10,** 434–441
7. Blake, D. R., Robson, P., Ho, M., Jubb, R. W., and McCabe, C. S. (2006) *Rheumatology* **45,** 50–52
8. Tomida, I., Azuara-Blanco, A., House, H., Flint, M., Pertwee, R. G., and Robson, P. J. (2006) *J. Glaucoma* **15,** 349–353
9. Wang, T., Collet, J. P., Shapiro, S., and Ware, M. A. (2008) *Can. Med. Assoc. J.* **178,** 1669–1678
10. Matsuda, L. A., Lolait, S. J., Brownstein, M. J., Young, A. C., and Bonner, T. I. (1990) *Nature* **346,** 561–564
11. Munro, S., Thomas, K. L., and Abu-Shaar, M. (1993) *Nature* **365,** 61–65
12. Baker, D., Pryce, G., Davies, W. L., and Hiley, C. R. (2006) *Trends Pharmacol. Sci.* **27,** 1–4
13. Walter, L., and Stella, N. (2004) *Br. J. Pharmacol.* **141,** 775–785
14. Galiègue, S., Mary, S., Marchand, J., Dussossoy, D., Carrière, D., Carayon, P., Bouaboula, M., Shire, D., Le Fur, G., and Casellas, P. (1995) *Eur. J. Biochem.* **232,** 54–61
15. Lyman, W. D., Sonett, J. R., Brosnan, C. F., Elkin, R., and Bornstein, M. B. (1989) *J. Neuroimmunol.* **23,** 73–81
16. Palazuelos, J., Davoust, N., Julien, B., Hatterer, E., Aguado, T., Mechoulam, R., Benito, C., Romero, J., Silva, A., Guzmán, M., Nataf, S., and Galve-Roperh, I. (2008) *J. Biol. Chem.* **283,** 13320–13329
17. Galve-Roperh, I., Aguado, T., Palazuelos, J., and Guzmán, M. (2008) *Curr. Pharm. Des.* **14,** 2279–2288
18. Maresz, K., Pryce, G., Ponomarev, E. D., Marsicano, G., Croxford, J. L., Shriver, L. P., Ledent, C., Cheng, X., Carrier, E. J., Mann, M. K., Giovannoni, G., Pertwee, R. G., Yamamura, T., Buckley, N. E., Hillard, C. J., Lutz, B., Baker, D., and Dittel, B. N. (2007) *Nat. Med.* **13,** 492–497
19. Moynagh, P. N. (2005) *Trends Immunol.* **26,** 469–476
20. Medzhitov, R., Preston-Hurlburt, P., Kopp, E., Stadlen, A., Chen, C., Ghosh, S., and Janeway, C. A., Jr. (1998) *Mol. Cell* **2,** 253–258
21. Fitzgerald, K. A., McWhirter, S. M., Faia, K. L., Rowe, D. C., Latz, E., Golenbock, D. T., Coyle, A. J., Liao, S. M., and Maniatis, T. (2003) *Nat. Immunol.* **4,** 491–496
22. O'Brien, K., Fitzgerald, D. C., Naiken, K., Alugupalli, K. R., Rostami, A. M., and Gran, B. (2008) *Curr. Med. Chem.* **15,** 1105–1115
23. Bsibsi, M., Ravid, R., Gveric, D., and van Noort, J. M. (2002) *J. Neuropathol. Exp. Neurol.* **61,** 1013–1021
24. Curran, N. M., Griffin, B. D., O'Toole, D., Brady, K. J., Fitzgerald, S. N., and Moynagh, P. N. (2005) *J. Biol. Chem.* **280,** 35797–35806
25. Martin, M. U., and Wesche, H. (2002) *Biochim. Biophys. Acta* **1592,** 265–280
26. Touil, T., Fitzgerald, D., Zhang, G. X., Rostami, A., and Gran, B. (2006) *J. Immunol.* **177,** 7505–7509
27. Buenafe, A. C., and Bourdette, D. N. (2007) *J. Neuroimmunol.* **182,** 32–40
28. Downer, E. J., Cowley, T. R., Lyons, A., Mills, K. H., Berezin, V., Bock, E., and Lynch, M. A. (2010) *Neurobiol. Aging* **31,** 118–128
29. Smith, P., Fallon, R. E., Mangan, N. E., Walsh, C. M., Saraiva, M., Sayers, J. R., McKenzie, A. N., Alcami, A., and Fallon, P. G. (2005) *J. Exp. Med.* **202,** 1319–1325
30. Croxford, J. L., and Miller, S. D. (2003) *J. Clin. Invest.* **111,** 1231–1240
31. Wraith, D. C., Pope, R., Butzkueven, H., Holder, H., Vanderplank, P., Lowrey, P., Day, M. J., Gundlach, A. L., Kilpatrick, T. J., Scolding, N., and Wynick, D. (2009) *Proc. Natl. Acad. Sci. U.S.A.* **106,** 15466–15471
32. Nair, A., Frederick, T. J., and Miller, S. D. (2008) *Cell Mol. Life Sci.* **65,** 2702–2720
33. Prinz, M., Garbe, F., Schmidt, H., Mildner, A., Gutcher, I., Wolter, K., Piesche, M., Schroers, R., Weiss, E., Kirschning, C. J., Rochford, C. D., Brück, W., and Becher, B. (2006) *J. Clin. Invest.* **116,** 456–464
34. Guo, B., Chang, E. Y., and Cheng, G. (2008) *J. Clin. Invest.* **118,** 1680–1690
35. Taniguchi, T., Ogasawara, K., Takaoka, A., and Tanaka, N. (2001) *Annu. Rev. Immunol.* **19,** 623–655
36. Oshiumi, H., Matsumoto, M., Funami, K., Akazawa, T., and Seya, T. (2003) *Nat. Immunol.* **4,** 161–167
37. Servant, M. J., Grandvaux, N., tenOever, B. R., Duguay, D., Lin, R., and Hiscott, J. (2003) *J. Biol. Chem.* **278,** 9441–9447
38. Clément, J. F., Meloche, S., and Servant, M. J. (2008) *Cell Res.* **18,** 889–899
39. Wandinger, K. P., Wessel, K., Neustock, P., Siekhaus, A., and Kirchner, H. (1997) *J. Neurol. Sci.* **149,** 87–93
40. Stasiolek, M., Bayas, A., Kruse, N., Wieczarkowiecz, A., Toyka, K. V., Gold, R., and Selmaj, K. (2006) *Brain* **129**, 1293–1305
41. Kraus, J., Voigt, K., Schuller, A. M., Scholz, M., Kim, K. S., Schilling, M., Schäbitz, W. R., Oschmann, P., and Engelhardt, B. (2008) *Mult. Scler.* **14,** 843–852
42. Smith, S. R., Denhardt, G., and Terminelli, C. (2001) *Eur. J. Pharmacol.* **432,** 107–119
43. Ni, X., Geller, E. B., Eppihimer, M. J., Eisenstein, T. K., Adler, M. W., and Tuma, R. F. (2004) *Mult. Scler.* **10,** 158–164
44. Siednienko, J., Halle, A., Nagpal, K., Golenbock, D. T., and Miggin, S. M. (2010) *Eur. J. Immunol.* **40,** 3150–3160
45. O'Sullivan, S. E. (2007) *Br. J. Pharmacol.* **152,** 576–582
46. Facchinetti, F., Del Giudice, E., Furegato, S., Passarotto, M., and Leon, A. (2003) *Glia* **41,** 161–168
47. Germain, N., Boichot, E., Advenier, C., Berdyshev, E. V., and Lagente, V. (2002) *Int. Immunopharmacol.* **2,** 537–543
48. Nilsson, O., Fowler, C. J., and Jacobsson, S. O. (2006) *Eur. J. Pharmacol.* **547,** 165–173
49. Smith, S. R., Terminelli, C., and Denhardt, G. (2000) *J. Pharmacol. Exp. Ther.* **293,** 136–150
50. Rizzo, V., Ferraro, G., Carletti, F., Lonobile, G., Cannizzaro, C., and Sardo, P. (2009) *Neurosci. Lett.* **462,** 135–139
51. Pohl, D. (2009) *J. Neurol. Sci.* **286,** 62–64

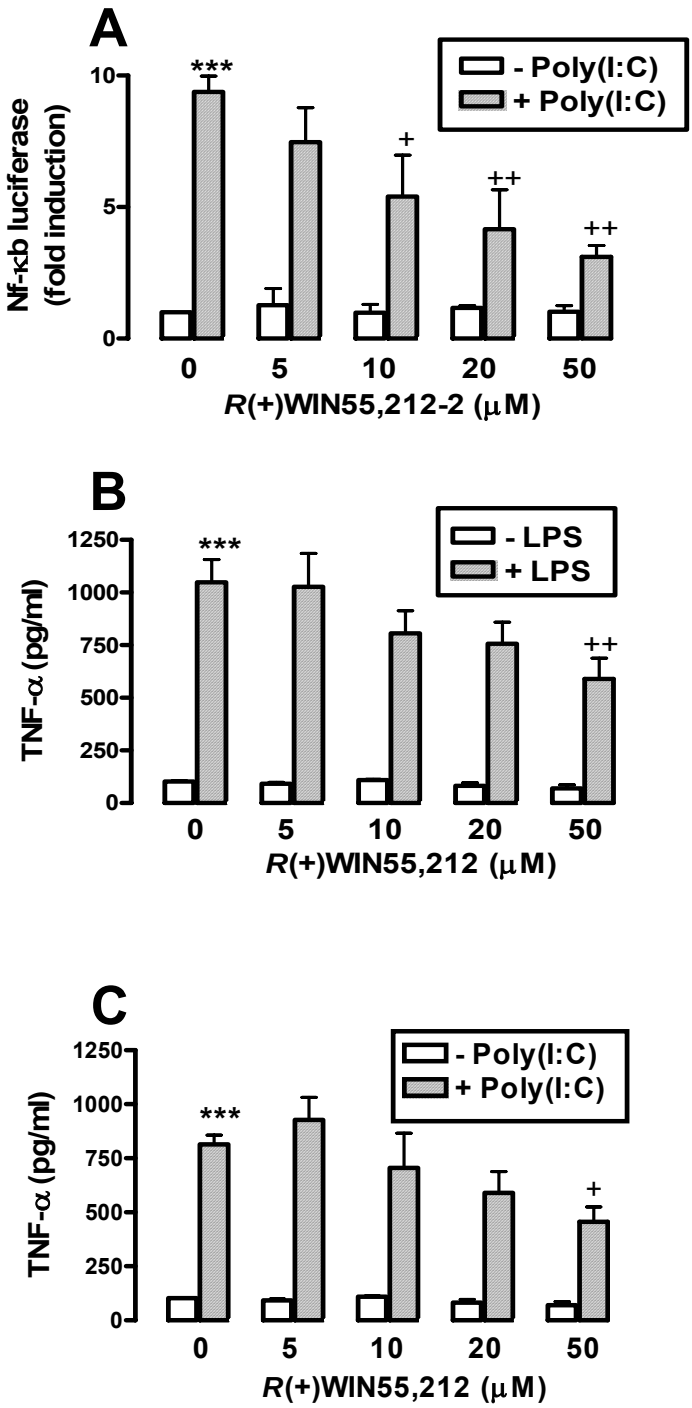

Supplemental Fig. 1.

***R*(+)WIN55,212-2 negatively regulates the NF-κB-regulated reporter gene and TNF-α production following TLR3/4 stimulation in U373-CD14 astrocytoma cells.** (*A*) Effect of *R*(+)WIN55,212-2 on Poly(I:C)-induced NF-κB luciferase activity in U373-CD14 cells (6 h; $n = 2$). Effect of *R*(+)WIN55,212-2 (1 h pre-treatments) on (*B*) LPS and (*C*) Poly(I:C) induction of TNF-α in U373-CD14 cells (6 h; $n = 3$). ***$p < 0.001$ compared with vehicle-treated cells. $^{+}p < 0.05$ and $^{++}p < 0.01$ compared with LPS or Poly(I:C)-treated cells. All values are mean ± SEM and are representative of 2-3 independent experiments.

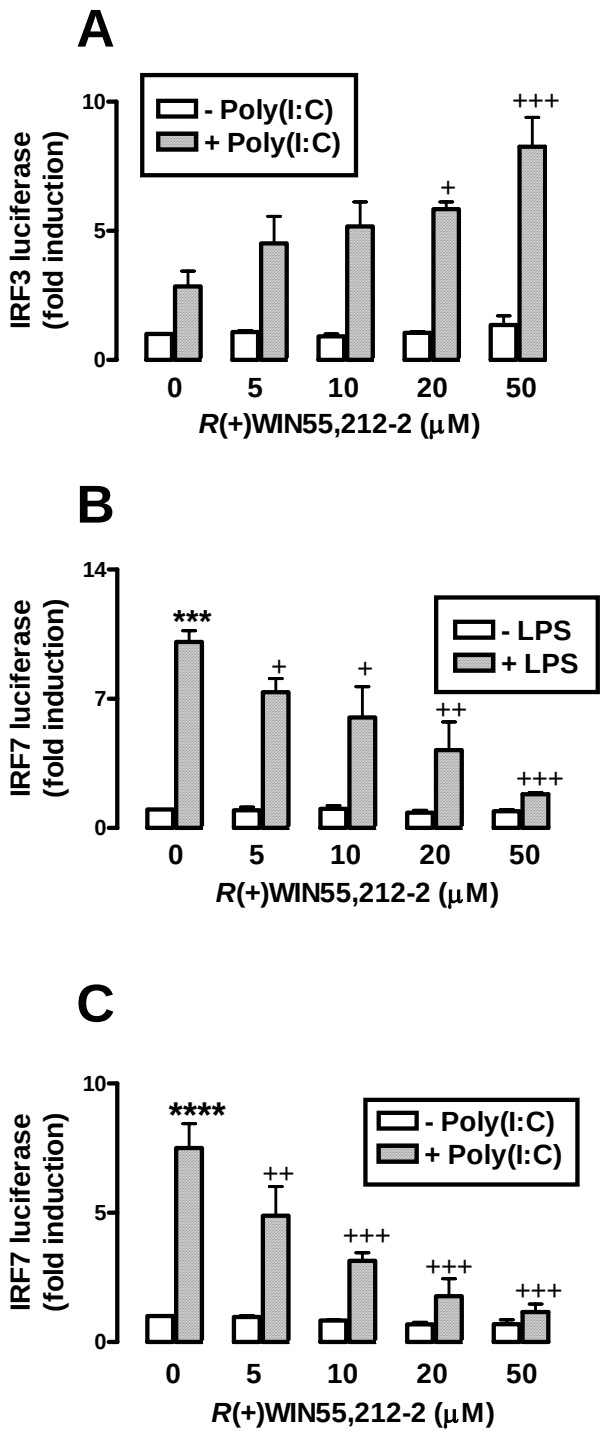

Supplemental Fig. 2.
Effect of *R*(+)WIN55,212-2 on TLR3- and TLR4-induced activation of IRF3 and IRF7 transcription factors in U373-CD14 cells. (*A*) Effect of *R*(+)WIN55,212-2 (1 h pre-treatment) on Poly(I:C)-induced activation of IRF3 luciferase in U373-CD14 cells (6 h; $n = 2$). Effect of *R*(+)WIN55,212-2 (1 h pre-treatments) on (*B*) LPS- and (*C*) Poly(I:C)-induced activation of IRF7 luciferase in U373-CD14 cells (6 h; $n = 2$). ***$p < 0.001$ compared with vehicle-treated cells. $^{+}p < 0.05$, $^{++}p < 0.01$ and $^{+++}p < 0.001$ compared with LPS or Poly(I:C)-treated cells. All values are mean ± SEM and are representative of 2-3 independent experiments.

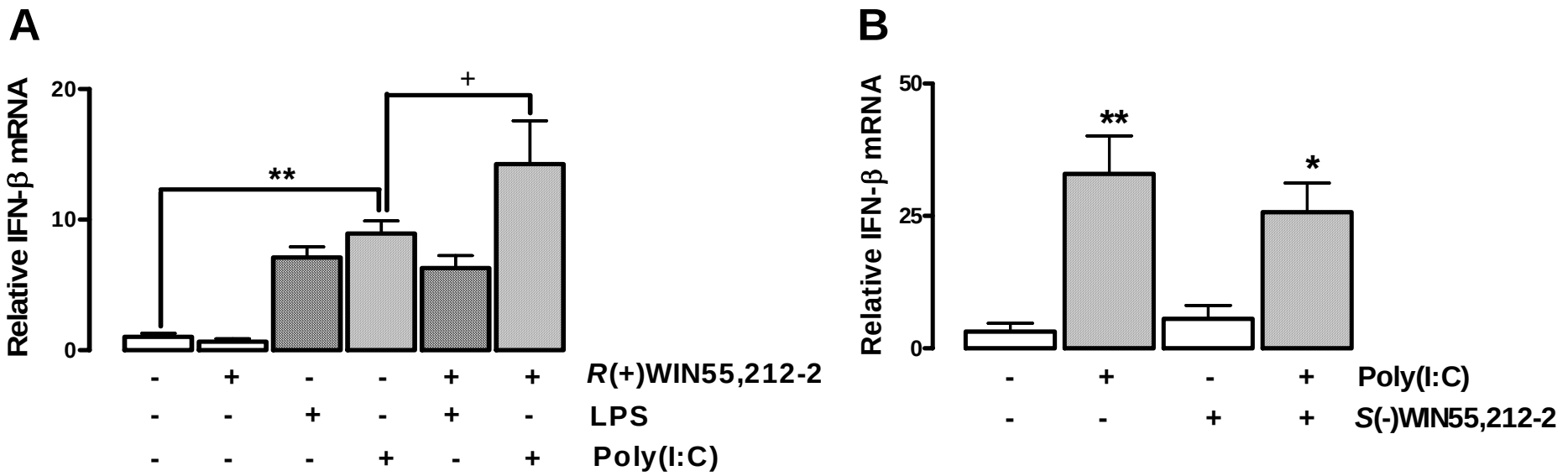

Supplemental Fig. 3.

***R*(+)WIN55,212-2 potentiates TLR3 induction of IFN-β in astrocytes.** (*A*) Effect of *R*(+)WIN55,212-2 (1 h pre-treatment) on LPS and Poly(I:C) induction of IFN-β mRNA in primary mouse astrocytes (4 h; $n = 9$). (*B*) Effect of *S*(-)WIN55,212-2 (1 h pre-treatment) on Poly(I:C) induction of IFN-β mRNA in primary mouse astrocytes (4 h; $n = 5$). *$p < 0.05$ and **$p < 0.01$ compared with vehicle-treated cells. $^{+}p < 0.05$ compared with Poly(I:C)-treated cells. All values are mean ± SEM and are representative of 2-3 independent experiments.

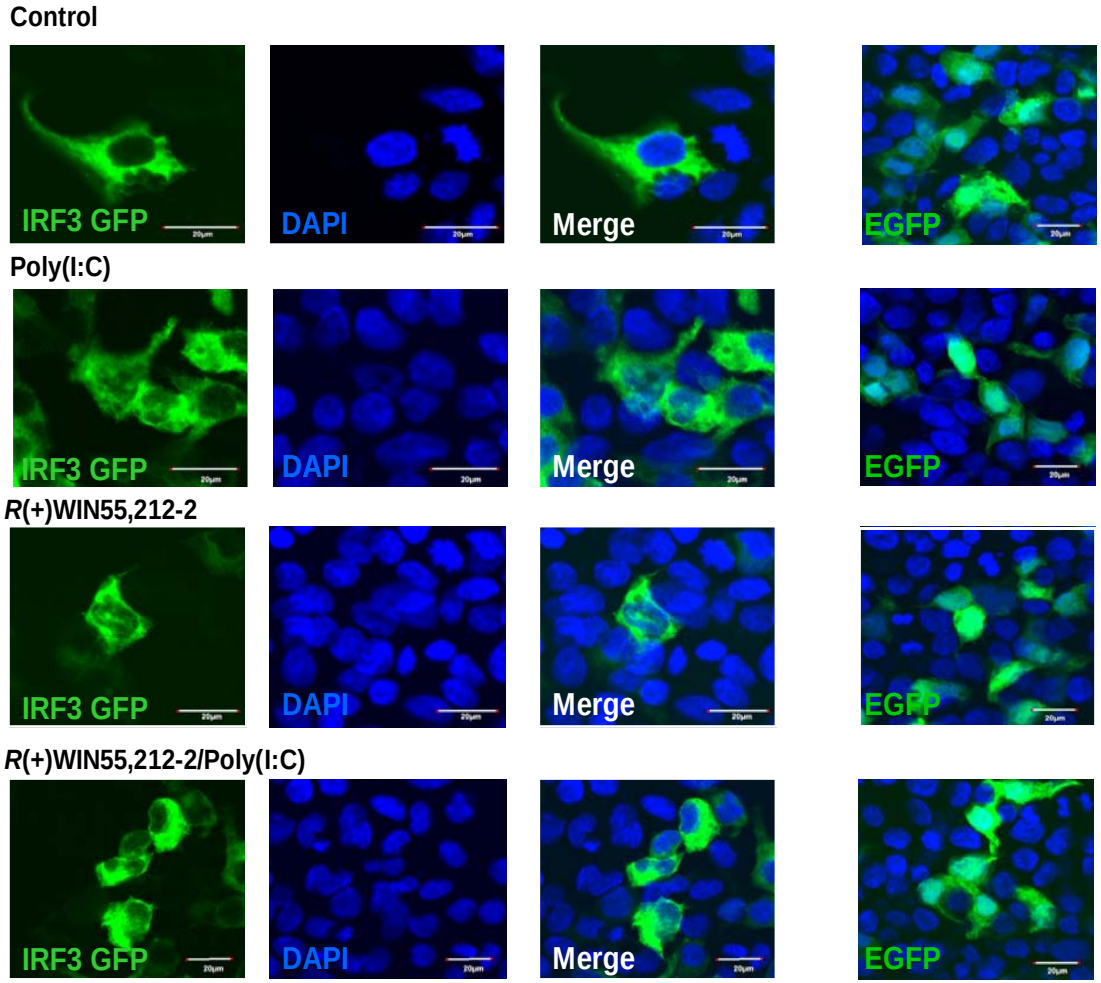

Supplemental Fig. 4. *R*(+)WIN55,212-2 promotes IRF3 translocation to the nucleus in HEK293-TLR3 cells. HEK293-TLR3 cells were seeded (1.5 x 10^5 cells/ml) in 4 well chamber slides for 24 h and transfected using Lipofectamine 2000 with an expression construct encoding GFP-tagged IRF3 (800 ng). Control slides were transfected with EGFP construct (800 ng). The following day cells were pre-treated with *R*(+)WIN55,212-2 (20 µM) 1 h prior to Poly(I:C) (25 µg/ml) exposure for 1 h. Cells were fixed in 4% PFA, incubated with DAPI (1.5 µg/ml) in PBS for 30 min, washed, and mounted (Vectashield; Vector Laboratories). All samples were viewed using an Olympus FluoView FV1000 confocal laser scanning microscope equipped with the appropriate filter sets. Acquired images were analysed using the Olympus FV-10 ASW imaging software. Images are represented of data from three independent experiments. Control EGFP is demonstrated in HEK293-TLR3 cells. Scale bars are 20 µm.